Quorum Regulation via Nested Antagonistic Feedback Circuits Mediated by the Receptors CD28 and CTLA-4 Confers Robustness to T Cell Population Dynamics

Zenke, S.; Palm, M.M.; Braun, J.; Gavrilov, A.; Meiser, P.; Bottcher, J.P.; ... ; Rohr, J.C.

Article

Immunity

Quorum Regulation via Nested Antagonistic Feedback Circuits Mediated by the Receptors CD28 and CTLA-4 Confers Robustness to T Cell Population Dynamics

Graphical Abstract

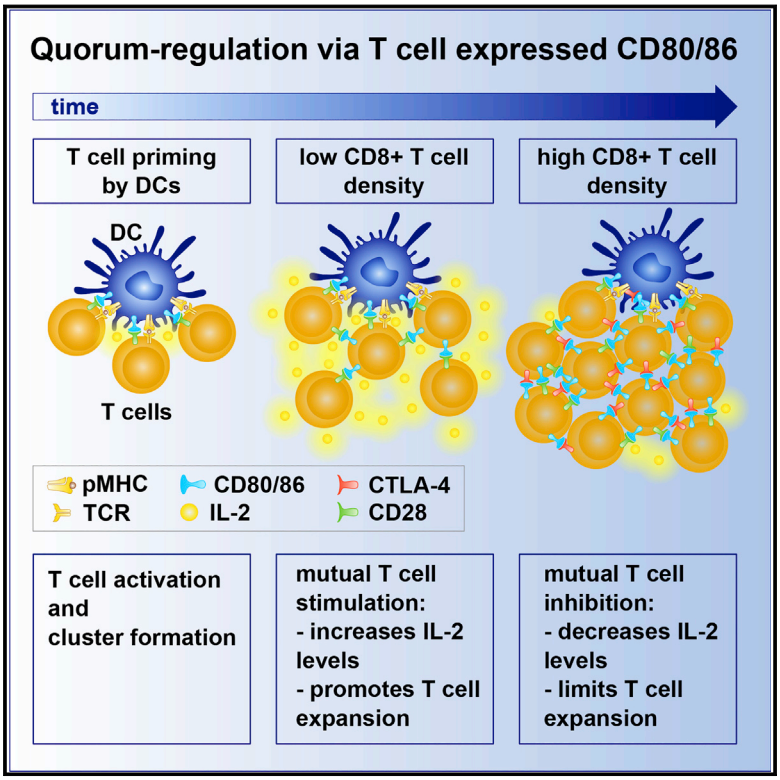

Highlights

- T cell clusters are communication hubs for coordination of population dynamics
- T cells can regulate their own population dynamics akin to quorum regulation
- T cell quorum regulation incorporates two nested antagonistic feedback circuits
- Loop dominance of feedback circuits is controlled by local T cell density

Authors

Simon Zenke, Margriet M. Palm, Julia Braun, ..., Ton N. Schumacher, Joost B. Beltman, Jan C. Rohr

Correspondence

jan.rohr@uniklinik-freiburg.de

In Brief

Zenke et al. show that dynamics of activated CD8+ T lymphocytes are shaped by intercellular communication in a manner akin to quorum regulation. Specifically, a network of nested antagonistic feedback circuits functions to sustain or curtail T cell expansion based on cellular density, thereby promoting robustness of T cell population dynamics.

Zenke et al., 2020, Immunity *52*, 313–327
February 18, 2020
https://doi.org/10.1016/j.immuni.2020.01.018

CellPress

Immunity
Article

Quorum Regulation via Nested Antagonistic Feedback Circuits Mediated by the Receptors CD28 and CTLA-4 Confers Robustness to T Cell Population Dynamics

Simon Zenke,[1,2,9] Margriet M. Palm,[3,9] Julia Braun,[1,2] Alina Gavrilov,[4] Philippa Meiser,[5] Jan P. Böttcher,[5] Niklas Beyersdorf,[6] Stephan Ehl,[1] Audrey Gerard,[7] Tim Lämmermann,[4] Ton N. Schumacher,[8] Joost B. Beltman,[3] and Jan C. Rohr[1,10,*]

[1]Institute for Immunodeficiency, Medical Center and Faculty of Medicine, Albert-Ludwigs University, Freiburg, Germany
[2]Faculty of Biology, Albert-Ludwigs University, Freiburg, Germany
[3]Division of Drug Discovery and Safety, Leiden Academic Centre for Drug Research, Leiden University, Leiden, the Netherlands
[4]Immune Cell Dynamics Group, Max Planck Institute of Immunobiology and Epigenetics, Freiburg, Germany
[5]Institute of Molecular Immunology and Experimental Oncology, School of Medicine, Klinikum rechts der Isar, Technical University of Munich, Munich, Germany
[6]Institute for Virology and Immunobiology, University of Würzburg, Würzburg, Germany
[7]The Kennedy Institute of Rheumatology, University of Oxford, Oxford, UK
[8]Division of Molecular Oncology and Immunology, Oncode Institute, the Netherlands Cancer Institute, Amsterdam, the Netherlands
[9]These authors contributed equally
[10]Lead Contact
*Correspondence: jan.rohr@uniklinik-freiburg.de
https://doi.org/10.1016/j.immuni.2020.01.018

SUMMARY

T cell responses upon infection display a remarkably reproducible pattern of expansion, contraction, and memory formation. If the robustness of this pattern builds entirely on signals derived from other cell types or if activated T cells themselves contribute to the orchestration of these population dynamics—akin to bacterial quorum regulation—is unclear. Here, we examined this question using time-lapse microscopy, genetic perturbation, bioinformatic predictions, and mathematical modeling. We found that ICAM-1-mediated cell clustering enabled CD8$^+$ T cells to collectively regulate the balance between proliferation and apoptosis. Mechanistically, T cell expressed CD80 and CD86 interacted with the receptors CD28 and CTLA-4 on neighboring T cells; these interactions fed two nested antagonistic feedback circuits that regulated interleukin 2 production in a manner dependent on T cell density as confirmed by *in vivo* modulation of this network. Thus, CD8$^+$ T cell-population-intrinsic mechanisms regulate cellular behavior, thereby promoting robustness of population dynamics.

INTRODUCTION

Upon different infections, pathogen-specific conventional T cells expand, contract, and form memory cells. The changes in population size underlying this pattern are determined by cell division and death rates at different points in time (Heinzel et al., 2017; Li et al., 2017). Division outweighs death during T cell expansion, but this ratio turns at the onset of contraction and equilibrates during the memory phase. In a simple tug-of-war scenario between division and death, population kinetics would be unstable with a high likelihood of population extinction or persistent growth. Remarkably, for any infection the dynamic pattern of T cell responses, including memory formation, is quite reproducible across biological replicates. How is robustness conferred to T cell dynamics in light of their regulation by cell division and death?

Using different single-cell tracking methods, we and others have demonstrated a striking diversity in clonal expansion of individual naive CD8$^+$ T cells (Buchholz et al., 2013; Gerlach et al., 2013). As a consequence of this diversity, robustness of T cell responses is only observed at the population level through summation of heterogenous single-cell behaviors. However, if individual T cells act independently of each other or if their behaviors are coordinated is not clear. Our understanding of the regulation of T cell responses is largely focused on mechanisms that are extrinsic to the population of conventional T cells. For example, signals provided by dendritic cells (DCs) and regulatory T (Treg) cells are able to stimulate and restrain, respectively, conventional T cells. However, such population-extrinsic control of T cell responses is prone to variability, because tailoring the strength of extrinsic regulatory signals to the size of the population regulated is challenging. In contrast, if members of a population mutually control each other, the strength of regulatory signals scales with the population size. Hence, if conventional T cells themselves coordinated behavior at a population level, this would promote robustness. Importantly, population-intrinsic and -extrinsic regulation are not mutually exclusive. This means that a layer of regulation intrinsic to conventional T cells could integrate extrinsic signals provided by DCs and Treg cells. For T cells, population-intrinsic control mechanisms are ill defined, although it is known that they can emanate signals that affect the behavior of neighboring T cells

(Gérard et al., 2013; Sabatos et al., 2008; Voisinne et al., 2015). Still, it is largely unclear if broadcasting such signals is a default program of T cell activation or if T cells modulate such communication to mutually regulate their behavior.

A prototype for population-intrinsic behavioral control is bacterial quorum regulation (Waters and Bassler, 2005). It builds on the ability of population members to mutually sense each other and adjust their behavior accordingly. This enables collective decision making based on cellular abundance, density, and activation state, allowing the population to act as a multicellular entity. Notably, quorum regulation relies on neither hierarchical nor mutual regulation of different cell types but instead on self-organization within a population. Quorum regulation programs population dynamics despite heterogeneity of individual cells and actually integrates this variability as an essential component of population control, as identical behavior of all cells would lead to population extinction at the moment the death rate outweighed the division rate (You et al., 2004).

Quorum regulation frequently integrates mechanisms conferring robustness to dynamic systems, such as niche formation, intercellular communication (You et al., 2004), and feedback (Chen et al., 2013). Niches provide sheltered spaces where cells experience similar conditions. In addition, niches facilitate intercellular communication and thereby enable orchestration of multicellular behaviors. Accordingly, linking intercellular communication to cell survival can confer population stability (You et al., 2004). In quorum-regulated systems, the strength of signals exchanged typically depends on cellular abundance and density and is subject to feedback control. Whereas signal responses are amplified by positive and dampened by negative feedback circuits, interlacing of positive and negative feedback stabilizes dynamic systems. Several studies have found that cellular abundance or density play a role in shaping T cell behavior (Bosch et al., 2017; Bretscher, 1999; Polonsky et al., 2018), but whether or not T cell responses fulfill all the hallmarks of quorum-regulated systems and if so, what mechanisms underlie such regulation, is still unclear.

Here, we investigated whether activated $CD8^+$ T cells employ quorum regulation to modulate their population dynamics. *In vivo*, $CD8^+$ T lymphocytes interact with multiple cell types. This makes it difficult to identify and characterize $CD8^+$ T cell population intrinsic control mechanisms. Therefore, we first employed reductionist *in vitro* systems allowing precise control over the cell types involved and subsequently demonstrated the *in vivo* relevance of these mechanisms. We found that clustering of activated T cells provided a niche for mutual behavioral coordination in a cell-count- and -density-dependent manner. $CD8^+$ T cells used CD80 and CD86 to drive two antagonistic feedback circuits via the shared receptors CD28 and CTLA-4 to self-regulate expansion dynamics. Costimulation via T cell-expressed CD80 and CD86 drove a CD28- and interleukin (IL)-2-mediated positive feedback circuit, promoting survival. CD80 and CD86 also induced CTLA-4 expression in an IL-2-mediated and cell-density-dependent manner, thereby creating a nested inhibitory feedback loop that limited T cell expansion. Mathematical modeling demonstrated that these feedback circuits quantitatively explain T cell population dynamics. Together, our data establish T cell clusters as communication hubs for quorum regulation of activated T cells and delineate the signals underlying this process.

RESULTS

Activated T Cells Self-Promote Cluster Formation, which Facilitates Mutual Interaction

Upon antigen encounter, T cells rapidly aggregate into cell clusters around DCs (Figure 1A) (Hommel and Kyewski, 2003; Khanna et al., 2007). Beyond the interaction with DCs, these niches could provide a spatiotemporal framework for T cell quorum regulation. In such a case, T cells might actively contribute to cluster formation rather than it being just a by-product of the interaction with DCs. The adhesion between T cells and DCs is mediated by the binding of T cell-expressed LFA-1 to DC-expressed ICAM-1 (Gérard et al., 2013; Zumwalde et al., 2013). Interestingly, upon priming by DCs, T cells also increased the expression of ICAM-1 (Figure 1B), which suggests that they also adhere to each other. To test this in a DC-free system, we exploited the fact that T cells can present antigens, e.g., those that they have acquired from DCs (Huang et al., 1999; Hudrisier et al., 2001). When we incubated purified P14 T cell receptor (TCR) transgenic $CD8^+$ T cells with the gp33 epitope recognized by this TCR, they still clustered and proliferated vigorously, indicating that T cells effectively presented antigen to each other (Figure 1C). We observed that upon activation, also purified T cells dynamically increased and later decreased both ICAM-1 and LFA-1 expression (Figures 1D and 1E) and that this mirrored the kinetics of cluster formation (Figure 1F; Video S1). As expected, blocking the ICAM-1:LFA-1 interaction abrogated T cell clustering (Figure 1F). These results demonstrate that antigen recognition rapidly puts T cells into a state in which they actively contact each other.

Activated T Cells Coexpress Multiple Receptor-Ligand Pairs

Clustering increases the efficiency of intercellular communication via soluble mediators and membrane-bound ligands. This raises the question how T cells exchange information. Conceptually, communication among T cells requires them to both send and receive specific signals and, thus, to coexpress receptors and corresponding ligands. To identify potentially relevant interactions, we developed a bioinformatic algorithm employing a library of approximately 1,500 receptor-ligand pairs to interrogate published transcriptome data of naive and activated $CD8^+$ T lymphocytes for coregulated receptor-ligand pairs. This enabled us to identify receptor-ligand pairs (1) that were expressed by T cells, (2) whose expression increased upon T cell activation, and (3) that were coregulated in multiple infection models. The approach identified multiple candidate interactions that have been implicated in communication among T cells, like IL-2:IL2R, interferon (IFN)γ:IFNγR and several chemokines, thereby validating our bioinformatic approach (Table S1) (Gérard et al., 2013; Hugues et al., 2007; Klebanoff et al., 2016; Sabatos et al., 2008).

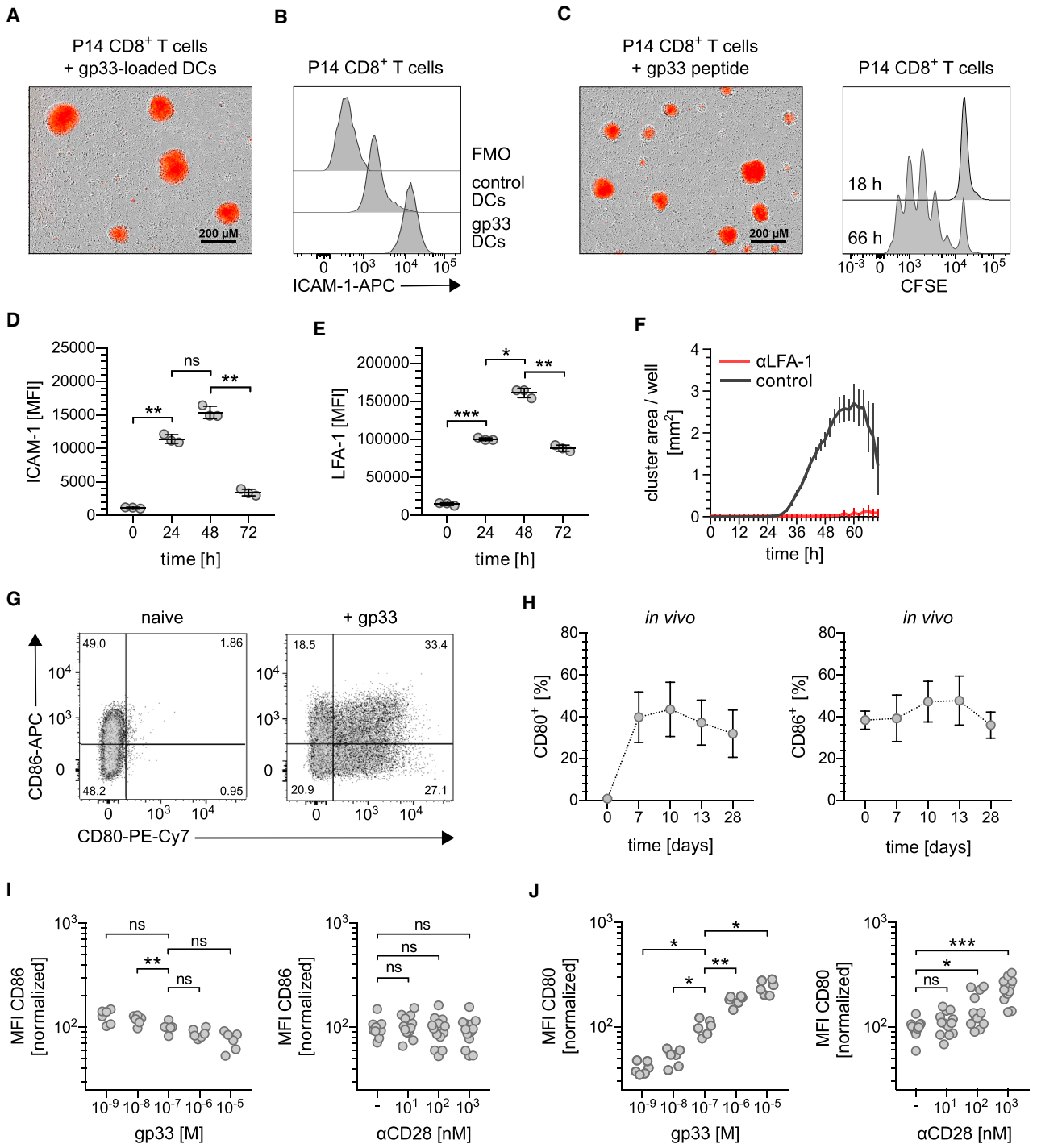

Figure 1. Activation-Induced T Cell Clustering, Expansion, and Expression of CD80

(A and B) Coculture of mTmG-P14 CD8$^+$ T cells with DCs loaded with the gp33 epitope recognized by the P14 TCR. Image of cell cluster formation (A) and flow cytometric quantification of ICAM-1 expression on P14 T cells (B). FMO, fluorescence minus one control stain.

(C–F) Analysis of mTmG-P14 CD8$^+$ T cells upon stimulation with gp33 only. Image of cell cluster formation (C, left), expansion of CFSE-labeled P14 T cells (C, right), T cell expression kinetics of ICAM-1 (D) and LFA-1 (E), and cluster area kinetics with and without LFA-1 blockade (F).

(G) CD80 and CD86 expression on naive and gp33-stimulated CD8$^+$ P14 T cells.

(H) Kinetics of CD80 and CD86 expression on adoptively transferred P14 T cells in blood upon LCMV infection.

(I and J) Expression of CD86 (I) and CD80 (J) on day 3 after activation with titrated doses of gp33 (left) or a fixed dose of 10^{-7} M gp33 and titrated doses of anti-CD28-antibody (right). To enable comparisons across multiple experiments, values were normalized to "10^{-7} M gp33 only" group per experiment. All data shown in this figure are from ≥3 independent experiments with 2–5 biological replicates each. Statistical tests: ANOVA (D, E, I, and J). Error bars depict mean ± SD. See also Video S1 and Table S1.

The algorithm also predicted CD80 and CD86 and their shared receptors CD28 and CTLA-4 as candidate receptor-ligand pairs for interactions among T cells. We chose to focus on these interactions, because the binding of CD80 and CD86 to either CD28 or CTLA-4 mediates costimulatory versus inhibitory effects, respectively, and could thus enable T cells to mutually stimulate and inhibit each other. In addition to their well-known function on DCs, CD80 and CD86 expression has been reported on T cells (Azuma et al., 1993; Prabhu Das et al., 1995), but the role of such expression has largely remained elusive. We thus investigated if these molecules enable T cells to mutually regulate their population dynamics. As the bioinformatic algorithm was based on mRNA expression, we first examined the protein expression of CD80 and CD86 on T cells. While up to 50% of naive $CD8^+$ T cells expressed CD86, CD80 was only expressed upon T cell activation both *in vitro* and *in vivo* (Figures 1G and 1H). Specifically, antigen recognition and CD28 co-stimulation drove CD80 expression in a dose-dependent manner, whereas they had little effect on CD86 (Figures 1I and 1J).

Mutual Costimulation of Activated T cells Regulates IL-2 Production

We next investigated the function of CD80 and CD86 within T cell clusters. The expansion of gp33-stimulated purified $CD8^+$ P14 T cells was abrogated when cluster formation was inhibited by LFA-1 blockade, but not when this was combined with CD28-stimulation (Figure 2A). Even when we did not block cluster formation, blockade of CD28 signaling diminished T cell expansion (Figure 2B). Likewise, $Cd80^{-/-}Cd86^{-/-}$ T cells failed to expand unless external CD28 stimulation through crosslinking was provided (Figure 2C). This deficit could not be overcome by increasing antigen concentrations (Figure S1A). Together, the observations that activated T cells clustered, expressed CD80 and CD86, and required ligation of CD28 for expansion in a setup where other CD80 or CD86 expressing cells are purposely absent are consistent with the hypothesis that LFA-1:ICAM-1-mediated cell clustering provides a scaffold for mutual costimulation of T cells. To directly test this, we cocultured P14 and P14 $Cd80^{-/-}Cd86^{-/-}$ T cells in the same well. In this setup, $Cd80^{-/-}Cd86^{-/-}$ T cells expanded comparably to wild-type (WT) T cells (Figure 2D). Despite the use of purified $CD8^+$ T cells in coculture experiments, the possibility remained that few residual WT professional antigen-presenting cells (APCs) drove the expansion of P14 and P14 $Cd80^{-/-}Cd86^{-/-}$ T cells. To exclude this, we used a setup where only T cells were able to express CD80 or CD86. We activated purified $CD8^+$ P14 $Cd80^{-/-}Cd86^{-/-}$ T cells with gp33 and, after 24 h, retrovirally transduced them with *Cd80* or *Cd86*. As upon gp33 addition, only T cells divided and retroviruses only integrated into dividing cells (Figures S1B and S1C), this setup confined CD80 and CD86 expression to T cells. Transduction of $Cd80^{-/-}Cd86^{-/-}$ T cells with *Cd80* or *Cd86* markedly improved their expansion, while transduction with GFP only or mutants of *Cd80* and *CD86* that do not bind CD28 (*Cd80* Y201A; Wu et al., 1997; *Cd86* Q35A; Peach et al., 1995) did not (Figure 2E). These results demonstrate that T cells are able to mutually support their expansion via ligation of CD28 on neighboring T cells, suggesting that they can complement the costimulatory function of professional APCs.

To investigate whether WT T cells promote the expansion of $Cd80^{-/-}Cd86^{-/-}$ T cells directly or indirectly, we cocultured them in transwells. This setup allowed both populations to exchange soluble mediators but prevented direct contact. We observed that WT T cells did not need to directly contact $Cd80^{-/-}Cd86^{-/-}$ T cells to promote their expansion (Figure 2F). Likewise, transfer of medium from activated WT T cells improved the expansion of $Cd80^{-/-}Cd86^{-/-}$ T cells (Figure S1D). Thus, interaction among WT T cells expressing CD80 and CD86 drives the secretion of a soluble mediator capable of enhancing $Cd80^{-/-}Cd86^{-/-}$ T cell expansion. Signaling downstream of the CD80 and CD86 ligand CD28 is known to promote expression of IL-2, IFNγ, and other cytokines (Lindstein et al., 1989; Thompson et al., 1989). When we blocked IL-2 in WT supernatant, this abrogated its ability to promote $Cd80^{-/-}Cd86^{-/-}$ T cell expansion, whereas blocking IFNγ had little effect (Figure S1D). Likewise, provision of IL-2, but not IFNγ, restored the impaired expansion of $Cd80^{-/-}Cd86^{-/-}$ T cells (Figure 2G). Corroborating a role for CD80 and CD86 in IL-2 production, we found that the supernatants of activated $Cd80^{-/-}Cd86^{-/-}$ T cells contained less IL-2 than WT samples (Figure 2H) and that CD28 stimulation increased IL-2 concentrations (Figure S1E). $Cd80^{-/-}Cd86^{-/-}$ T cells also expressed lower levels of the high-affinity IL-2Rα (CD25) (Figure 2H). Yet the expansion was not primarily limited by a reduced sensitivity for IL-2, as shown by the inability of transgenic *Cd25* expression to restore $Cd80^{-/-}Cd86^{-/-}$ T cell expansion (Figures 2I and 2J). These results demonstrate that by expressing CD80 and CD86, T cells are able to mutually support their expansion via CD28 and IL-2.

Interactions among Activated T Cells Regulate Cell Survival

Population dynamics depend on division and survival rates. T cell division is controlled by Myc, whose expression depends on antigen and CD28- and IL-2-mediated signals (Heinzel et al., 2017). This suggests that expression of CD80, CD86, and IL-2 enables T cells to tune the division rates of neighboring T cells. In addition, we observed that CD28 and IL-2 increased the expression of the anti-apoptotic proteins Bcl-xL and Bcl-2, respectively, and inhibited cell death (Figures 3A and S1F). This indicates that T cells also mutually regulate their survival. To dissect the relative contributions of division and survival we transduced $Cd80^{-/-}Cd86^{-/-}$ T cells with *Bcl-xL*, *Bcl-2* or *Myc*. In these experiments both anti-apoptotic molecules restored $Cd80^{-/-}Cd86^{-/-}$ expansion, while Myc did not (Figure 3B). Hence, a major effect of CD28 and IL-2 is to limit T cell apoptosis, which is consistent with a censorship function of cell death on cell division. Concordantly, we found comparable division patterns of P14 and P14 $Cd80^{-/-}Cd86^{-/-}$ T cells after 2 days but a strikingly reduced accumulation of divided $Cd80^{-/-}Cd86^{-/-}$ cells after 3 days, indicating that $Cd80^{-/-}Cd86^{-/-}$ cells did not survive (Figures 3C and 3D). In line with this, increased death of $Cd80^{-/-}Cd86^{-/-}$ T cells occurred after day 2 (Figure 3E), which could not be prevented by increased antigen concentrations (Figure 3F). Together, these results demonstrate that the expression of CD80 and CD86 enable T cells to mutually promote their survival via CD28-driven IL-2 production.

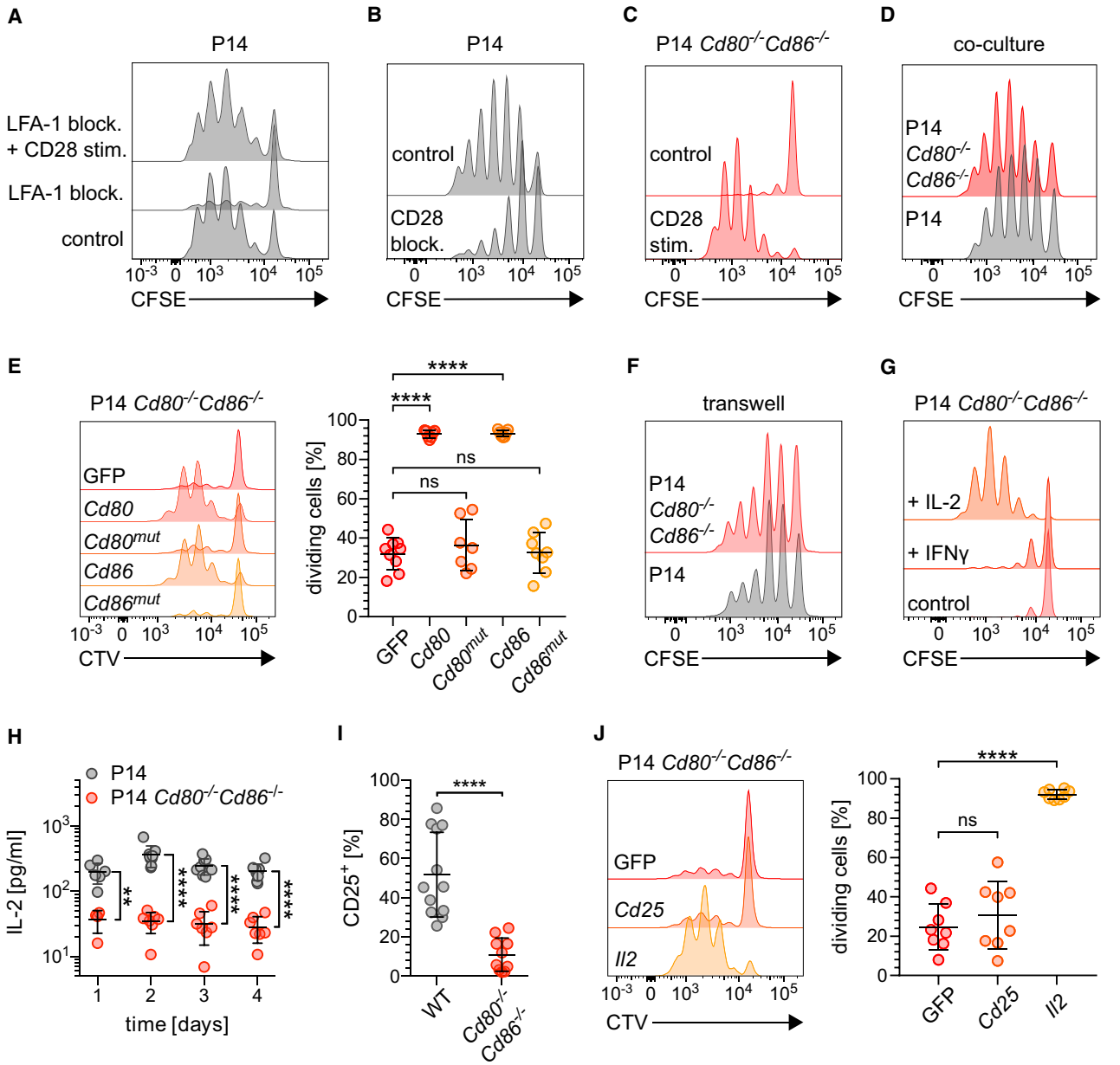

Figure 2. CD80 and CD86 Enable Mutual Costimulation of CD8⁺ T Cells via Increasing IL-2 Production

(A–D) Day 3 CFSE-proliferation profiles of gp33-stimulated, purified P14 CD8⁺ T cells upon LFA-1 blockade with or without agonistic anti-CD28 antibodies (A) and with or without blocking anti-CD28 Fab fragments (B), P14 *Cd80*$^{-/-}$*Cd86*$^{-/-}$ CD8⁺ T cells with or without crosslinking Anti-CD28 antibody (C), and co-cultured P14 and P14 *Cd80*$^{-/-}$*Cd86*$^{-/-}$ CD8⁺ T cells (D).

(E) Day 3 cell trace violet (CTV)-proliferation profiles (left) and quantification of divided cells (right) of purified, gp33-stimulated P14 *Cd80*$^{-/-}$*Cd86*$^{-/-}$ CD8⁺ T cells transduced with GFP, CD80, CD86, or mutants of CD80 or CD86, which are unable to bind CD28 and CTLA-4.

(F and G) Day 3 CFSE-proliferation profiles of gp33-stimulated, purified CD8⁺ P14 and P14 *Cd80*$^{-/-}$*Cd86*$^{-/-}$ T cells cultured in a transwell system (F) or of P14 *Cd80*$^{-/-}$*Cd86*$^{-/-}$ T cells with IL-2 or IFNγ supplementation (G).

(H) Kinetics of IL-2 concentration in supernatants of gp33-stimulated P14 and P14 *Cd80*$^{-/-}$*Cd86*$^{-/-}$ T cells.

(I) Day 2 proportions of gp33-stimulated P14 and P14 *Cd80*$^{-/-}$*Cd86*$^{-/-}$ T cells expressing the IL-2Rα chain (CD25).

(J) Day 3 CTV-proliferation profiles (left) and quantification of dividing cells (right) of purified, gp33-stimulated P14 *Cd80*$^{-/-}$*Cd86*$^{-/-}$ CD8⁺ T cells transduced with GFP, CD25, or IL-2.

Statistical tests: one-way ANOVA (E and J) and unpaired t test (H and I). All data shown in this figure are from ≥3 independent experiments with 2–3 biological replicates each. Error bars depict mean ± SD. See also Figure S1.

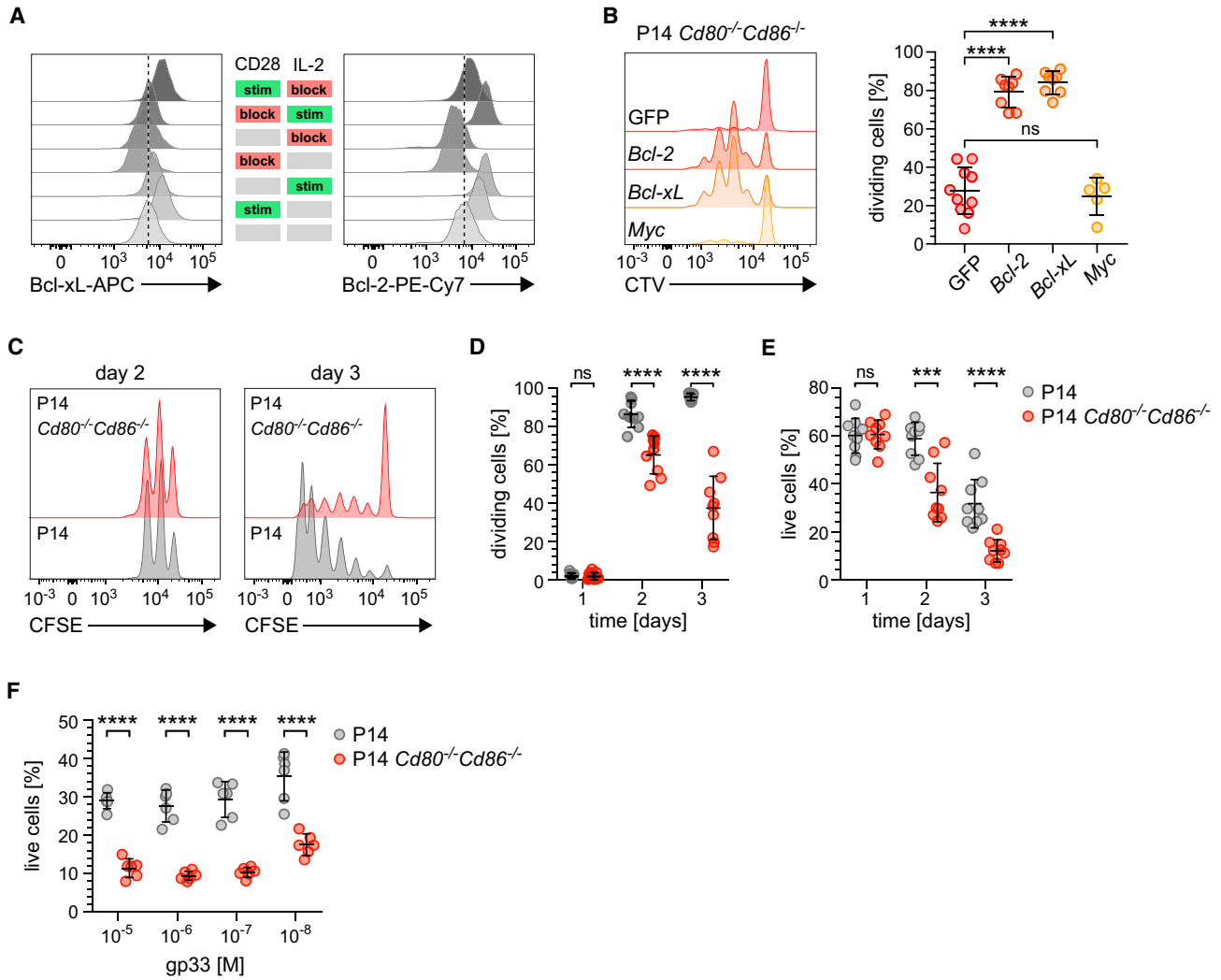

Figure 3. T Cell Interaction via CD80, CD86 and IL-2 Drives Cell Expansion by Inhibiting Apoptosis

(A) Day 2 expression of Bcl-xL and Bcl-2 in gp33 peptide-stimulated P14 T cells upon stimulation versus blockade of CD28 or IL-2.

(B) Day 3 CTV profiles (left) and quantification of divided cells (right) of gp33 peptide-stimulated P14 *Cd80*$^{-/-}$*Cd86*$^{-/-}$ T cells transduced with *GFP*, *Bcl-2*, *Bcl-xL*, or *Myc*.

(C–E) Comparative expansion (C and D) and survival (E) kinetics of gp33 peptide-stimulated P14 and P14 *Cd80*$^{-/-}$*Cd86*$^{-/-}$ T cells.

(F) Day 3 quantification of live cells of P14 and P14 *Cd80*$^{-/-}$*Cd86*$^{-/-}$ T cells stimulated with titrated concentrations of gp33 peptide.

Statistical tests: one-way ANOVA (B) and unpaired t test (D–F). All data shown in this figure are from ≥3 independent experiments with 2–3 biological replicates each. Error bars depict mean ± SD. See also Figure S1.

Activated T Cells Scale IL-2 Production According to Cell Density and Abundance

As signal intensity in quorum regulation generally depends on cellular density and abundance, we next investigated whether this also applies to IL-2. To modulate cell density, we activated T cells either in flat-bottom plates, where they arranged in a scattered distribution, or in u- or v-bottom plates, where gravity enforced close cellular proximity. When we seeded more than 5 × 10^4 $CD8^+$ T cells, carboxyfluoresceinsuccinimidylester (CFSE) patterns were similar across different plate types, indicating that cells were activated comparably (Figure S2A). Nevertheless, in u- and v-bottom plates, we detected significantly higher total and per-cell IL-2 concentrations than in flat-bottom plates (Figures 4A and S2B), demonstrating that the amount of IL-2 scales with T cell density. Furthermore, experiments where we seeded titrated numbers of T cells in u- (or v-) bottom plates indicated that at a given cell density IL-2 concentrations correlated linearly with cellular abundance (Figure 4B). As cluster formation increases cell density, these results show that T cell clustering itself and the size of clusters determine the abundance of IL-2, which is consistent with a role for IL-2 in T cell quorum regulation.

Nested Antagonistic Feedback Circuits Regulate T cell Clustering and Survival

Based on the notion that clustering enables T cells to mutually stimulate CD28-mediated IL-2 expression in a

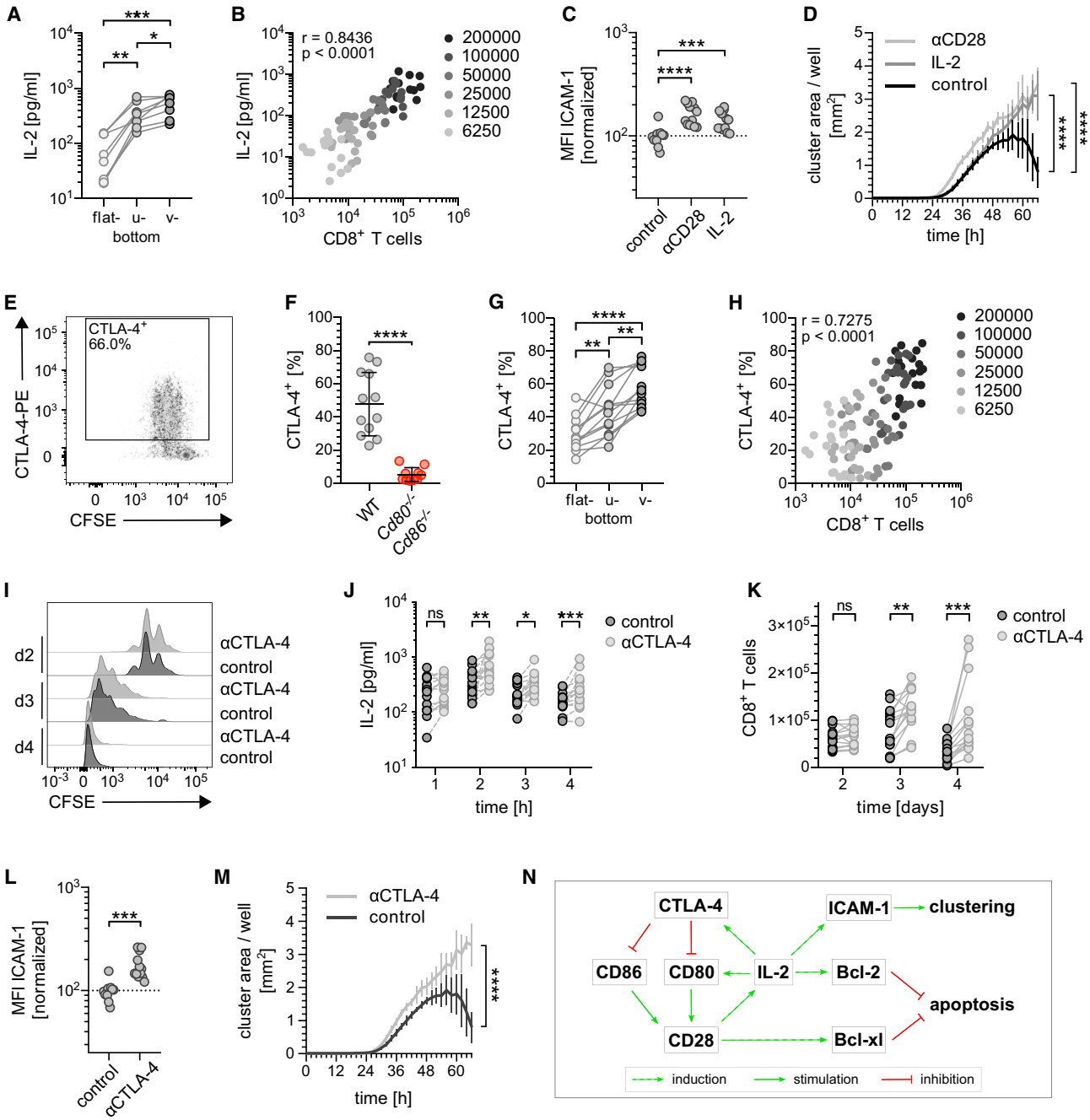

Figure 4. CD8$^+$ T Cell Quorum Regulation Operates via Nested Positive and Negative Feedback Circuits

(A) Day 2 IL-2 concentrations of 10^5 gp33-activated P14 T cells seeded in flat- versus u- versus v-bottom plates.

(B) Correlation of IL-2 concentrations and cell counts recovered on day 2 after seeding titrated numbers of gp33-activated P14 T cells in u-bottom plates.

(C) Day 2 ICAM-1 expression on gp33-activated P14 T cells with or without anti-CD28 antibodies or IL-2.

(D) Cluster area kinetics of gp33-activated P14 T cells with or without anti-CD28 antibodies or IL-2.

(E and F) Representative plot and quantification of CTLA-4 expression by gp33-activated P14 and P14 *Cd80*$^{-/-}$*Cd86*$^{-/-}$ T cells on day 2.

(G) Day 2 proportion of CTLA-4$^+$ cells of 10^5 gp33-activated P14 T cells seeded in flat- versus u- versus v-bottom plates.

(H) Correlation of cell counts recovered and proportion of CTLA-4$^+$ T cells on day 2 after seeding titrated numbers of gp33-activated P14 T cells in u-bottom plates.

(I–M) CFSE-profiles (I), IL-2 concentrations (J), cell counts recovered (K), ICAM-1 expression (L), and cluster area kinetics (M) of gp33-activated P14 T cells with or without anti-CTLA-4 antibodies.

(N) Scheme of CD8$^+$ T cell-intrinsic nested antagonistic feedback circuits regulated by CD80 and CD86.

Statistical tests: one-way ANOVA (A and G), Spearman log-rank test (B and H), ANOVA (C and L), unpaired t test (F), Wilcoxon matched pair (J and K), and ANOVA on area under curve (D and M). All data shown in this figure are from 3–8 independent experiments with 6 technical (D and M) or 2–3 biological replicates each (all other plots). Error bars depict mean ± SD. See also Figures S2 and S3 and Videos S2, S3, and S4.

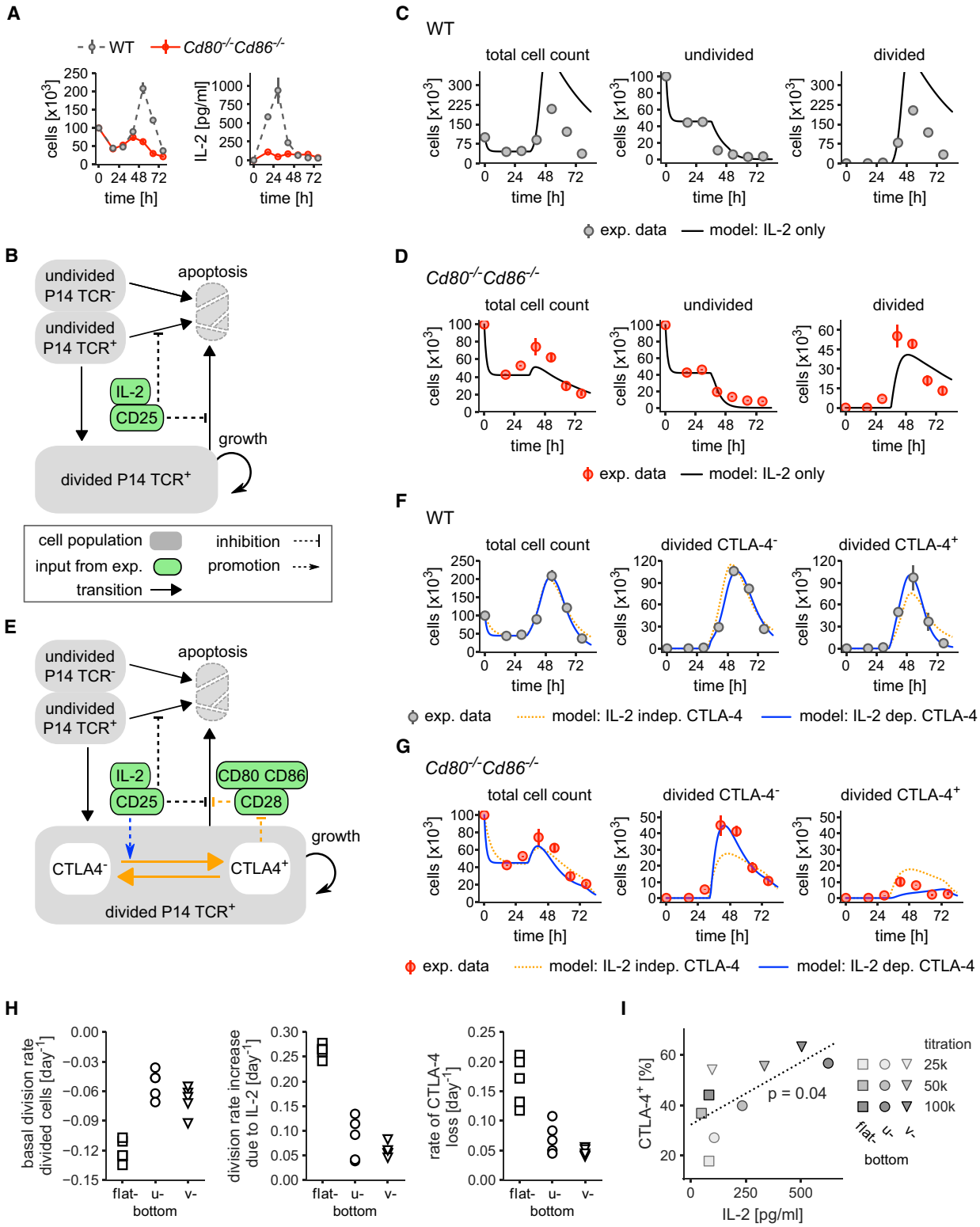

Figure 5. Mathematical Model Supports Regulation of T Cell Expansion by Nested Antagonistic Feedback Circuits

(A) Cell count (left) and IL-2 dynamics (right) for gp33 activated P14 WT (gray) and P14 *Cd80*$^{-/-}$*Cd86*$^{-/-}$ (red) T cells.

(B) Scheme of T cell expansion model regulated only by IL-2 and CD25.

(C and D) Overlays of best-fitting simulation for the model depicted in (B) and experimental data for WT (C) and *Cd80*$^{-/-}$*Cd86*$^{-/-}$ (D) cells.

(E) Scheme of T cell expansion model with IL-2R (black) and CD28 signaling (orange).

(legend continued on next page)

density-dependent manner, we investigated if in turn, CD28 and IL-2 modulate T cell cluster kinetics. We found that both signals increased ICAM-1 expression and inhibited cluster disaggregation (Figures 4C and 4D; Videos S2 and S3). Together with the pro-survival effects of CD28 and IL-2, these effects promote cluster growth, which again reinforces IL-2 and CD80 expression (Figures 4A, 4B, and S2C), thereby forming a positive feedback circuit driven by CD28 and IL-2. Unchecked activity of this circuit could result in self-perpetuation of T cell expansion. However, IL-2 concentrations peaked at day 2, and clusters dissolved shortly thereafter, pointing toward antagonistic mechanisms restricting IL-2 abundance and cluster growth. Notably, T cell expansion was not limited by the carrying capacity of the wells, as IL-2 addition yielded substantially higher cell counts (Figure S2D). A candidate molecule for such antagonistic mechanisms is CTLA-4, which was also predicted by our bioinformatic algorithm. CTLA-4 competes with CD28 for binding to CD80 and CD86, inhibits IL-2 expression, and induces T cell apoptosis (Gribben et al., 1995; Krummel and Allison, 1996; Scheipers and Reiser, 1998; Walunas et al., 1996). We observed substantial expression of CTLA-4 on activated $CD8^+$ T cells *in vitro* and *in vivo* (Figures 4E, S3A, and S3B), which was highest at contact sites of T cells within clusters (Figures S3C and S3D). Activated $Cd80^{-/-}Cd86^{-/-}$ T cells expressed very little CTLA-4, suggesting a stimulatory role for CD80 and/or CD86 on CTLA-4 expression (Figure 4F). Accordingly, both CD28 stimulation and IL-2 induced CTLA-4 expression (Figures S3E and S3F). CTLA-4 expression did not steadily increase with cell divisions or time, indicating that it functions as neither a division counter nor a timer (Figure S3G). Instead, CTLA-4 expression scaled with cell density and cell counts, thus mirroring IL-2 dynamics (Figures 4G and 4H). Addition of anti-CTLA-4 antibodies did not alter the cell division rate but increased IL-2 and ICAM-1 expression and, consequently, promoted cellular expansion and clustering (Figures 4I–4M; Video S4). Together, these experiments show that within cell clusters, T cell-expressed CD80 and CD86 feed two interlaced but antagonistic feedback circuits via CD28 and CTLA-4 (Figure 4N), with cell density shaping the relative activities of both circuits.

Antagonistic Feedback Loops Quantitatively Explain CD8+ T Cell Kinetics

To formally test if experimentally observed T cell dynamics can be explained by these intertwined antagonistic feedback loops, we constructed a dynamic mathematical model based on the abundances of receptors and ligands involved. We combined CFSE profiles with total cell-count quantification to deduce the dynamics of divided and undivided T cells (Figure 5A, left).

First, we tested if differences in IL-2-mediated effects alone sufficed to explain the different expansion kinetics observed for WT and $Cd80^{-/-}Cd86^{-/-}$ T cells (Figure 5A, right) by setting up a model in which the net growth rate (i.e., the net of division and death) solely depended on IL-2R signaling (Figure 5B). In the model, we interpolated dynamic measurements of IL-2 and CD25 expression as inputs that modify T cell expansion. As a subset of T cells did not express the P14 TCR and thus was not activated by gp33, we split the undivided cell population in P14 TCR^+ and P14 TCR^- cells. Fitting this model to experimental measurements indicated that it could reproduce the decline of undivided cells but not the population dynamics of divided cells (Figures 5C and 5D). We therefore included the stimulatory effect of the interaction of CD80 and CD86 with CD28 and the inhibitory effect of CTLA-4 into the model. Specifically, we considered the net growth rate of both populations to depend on IL-2R and CD28 signaling, with the latter being promoted by CD80 and CD86 and inhibited by CTLA-4. In the model, dividing cells initially did not express CTLA-4 but could gain or lose such expression over time. Since our data suggested that IL-2 drives CTLA-4 expression (Figure S3F), we implemented model variants with IL-2-independent and IL-2-dependent regulation of CTLA-4 dynamics (Figure 5E, black and orange lines versus black, orange, and blue lines, respectively). Fitting each model variant to WT and $Cd80^{-/-}Cd86^{-/-}$ cell data showed that IL-2-independent CTLA-4 regulation could reproduce total population dynamics but failed to describe the amount of $CTLA\text{-}4^+$ WT cells (Figure 5F), while the model variant with IL-2-dependent CTLA-4 expression closely matched the experimental data. Thus, our modeling confirms that the intertwined antagonistic feedback loops operating via CD28, IL-2R, and CTLA-4 are needed to quantitatively explain $CD8^+$ T cell population dynamics.

We next tested whether the model was also compatible with experiments initialized with titrated cell counts and different well shapes. The model fitted data for titrated cell counts with identical parameter values, indicating that it accurately captured effects of population size (Figure S4). It was also able to reproduce population dynamics of titrated cell counts across different well types (Figures S4 and S5). However, as cell density was not an input variable in the model, this required adjusting several parameters (Figure 5H). Notably, these adjustments identified parameters that depend on cell density. Specifically, they predicted that cell density affected the basal cell expansion rate and its increase upon IL-2R signaling. Both support the notion that direct contact enables T cells to promote their expansion (via mutual stimulation of CD28). Consistent with our experimental data, the model also predicted that CTLA-4 expression depends on cell density.

As CTLA-4 counteracts CD28- and IL-2-driven T cell expansion, it is unclear if the transition from population expansion to contraction is linked to a single CTLA-4 expression threshold. The model allowed us to refute this by revealing markedly

(F and G) Overlays of best-fitting simulations for two model variants with IL-2 independent (orange) and IL-2 dependent (blue) CTLA-4 expression and experimental data for WT (F) and $Cd80^{-/-}Cd86^{-/-}$ (G) cells.

(H) Five best fits of parameters found to be cell-density dependent.

(I) Fraction of $CTLA\text{-}4^+$ cells and IL-2 concentrations at the transition from population expansion to contraction of WT cells. Dotted line represents the linear regression.

Model parameters were obtained by fitting each model to experimental data of 10^5 input cells in flat-bottom wells (C, D, and F) or 0.25×, 0.5×, or 1 × 10^5 input cells in flat-, u-, or v-bottom wells (H and I) and are listed in Supplemental Information. Error bars depict SD of three technical replicates. See also Figures S3, S4, and S5.

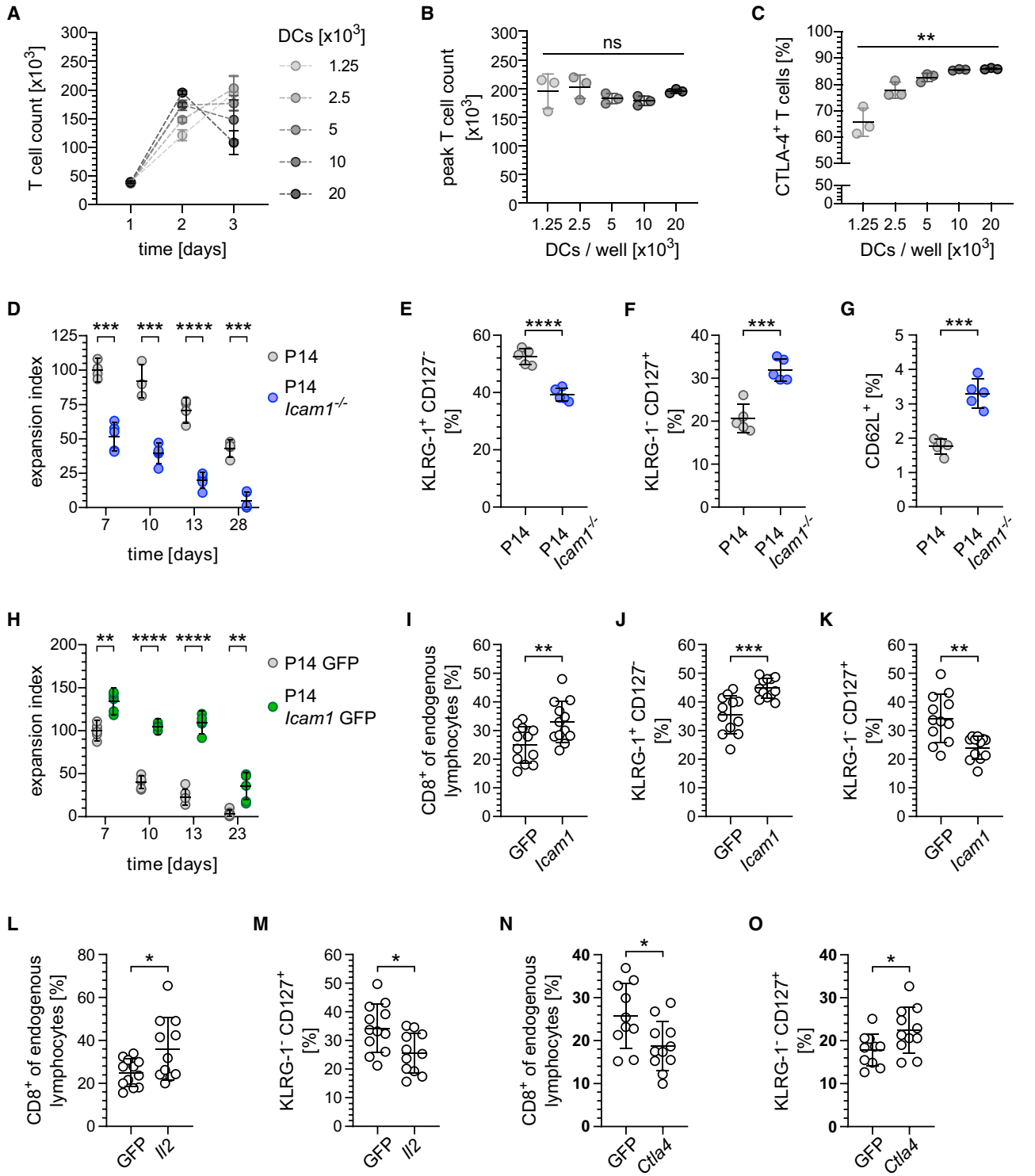

Figure 6. Mutual Regulation of CD8⁺ T Cells upon DC Priming *In Vitro* and *In Vivo*

(A–C) Coculture of 10^5 CD8⁺ P14 T cells with titrated amounts of gp33-loaded DCs. (A) Kinetics of T cell counts. (B) Peak T cell counts. (C) Day 2 CTLA-4 expression on T cells.

(D–G) Blood kinetics (D) and day 11 phenotype (E–G) of 500–800 adoptively transfered P14 or P14 *Icam1*$^{-/-}$ T cells upon LMCV infection. To allow for a comparision across experiments, T cell expansion was normalized to input cell counts with mean expansion of control group cells set to 100% (= expansion index).

(legend continued on next page)

differing CTLA-4 expressions at this transition for different cell counts and densities (Figure 5I). However, there was a direct correlation between IL-2 and CTLA-4 at the transition, indicating that the onset of population contraction is determined by both regulators. As the expression of IL-2 and CTLA-4 is functionally linked, these results provide a mechanism conferring robustness to population dynamics across different cell counts and densities.

T Cell Quorum Regulation Shapes T Cell Behavior upon Activation by DCs

So far, we have demonstrated the existence of T cell quorum regulation in a reductionist system employing T cells as APCs. Next, we investigated if this layer of regulation also modulated T cell expansion upon activation by DCs. To vary the strength of DC-mediated signals, we added titrated amounts of peptide-loaded DCs to $CD8^+$ T cells. Indeed, increased DC counts accelerated T cell expansion (Figures 6A and S6A). In the absence of T cell quorum regulation, the extent of T cell expansion would be expected to scale with the number of DCs. However, the peaks of T cell numbers and cluster area were both comparable despite variation in activation signals provided by DCs (Figures 6B and S6B). While this suggested a DC-extrinsic factor limiting T cell expansion, it was not due to cell counts reaching the carrying capacity of the wells (Figure S6C). Rather, T cells increased CTLA-4 expression with rising numbers of DCs (Figure 6C), pointing toward a role for T cells in dampening their own population dynamics. Together, these results indicate that also upon priming by DCs, T cells can regulate their population dynamics by integrating extrinsic signals into quorum regulation.

Next, we searched for evidence of mutual regulation of $CD8^+$ T cells *in vivo*. As T cell clustering provided a scaffold for quorum regulation, we asked whether modulating the capability of T cells to cluster altered their behavior upon infection with lymphocytic choriomeningitis virus (LCMV). Notably, while T cell expression of ICAM-1 is crucial for their clustering *in vivo*, it is dispensable for their activation by DCs (Gérard et al., 2013; Zumwalde et al., 2013). We observed that upon infection, the expansion of adoptively transferred P14 *Icam1*$^{-/-}$ T cells was curtailed to about 50% of control P14 T cells (Figure 6D). Furthermore, *Icam1*$^{-/-}$ P14 T cells expressed less KLRG-1 and more CD127 and CD62L (Figures 6E–6G). These observations corroborated our *in vitro* results indicating that T cell clustering led to more IL-2 exposure, because IL-2 has been shown to promote T cell expansion and KLRG-1-expression, and to inhibit CD127 and CD62L expression (Pipkin et al., 2010). Consistent with this interpretation, *Icam1*-transgenic P14 T cells expanded more strongly than control P14 T cells (Figure 6H).

For $CD8^+$ T cell quorum regulation operating *in vivo*, transferred P14 cells are expected to also impact on the behavior of endogenous, polyclonal $CD8^+$ T cells. Accordingly, we found that transfer of *Icam1*-transgenic P14 T cells also supported the expansion of endogenous $CD8^+$ T cells and shifted their differentiation toward a $KLRG1^+$ $CD127^-$ phenotype (Figures 6I–6K). We then tested if we could corroborate this observation using other elements of the identified feedback circuits. Indeed, adoptive transfer of *Il2* transgenic P14 T cells mimicked the effect of transferring *Icam1* transgenic P14 T cells (Figures 6L and 6M). Conversely, *Ctla4* transgenic P14 T cells suppressed the expansion of endogenous, polyclonal T cells and promoted their expression of CD127 (Figures 6N and 6O). Together, our observations establish that also *in vivo* $CD8^+$ T cells do not act entirely independent of each other but coordinate their behavior. Specifically, they demonstrate that altering the clustering capabilities of activated T cells *in vivo* modulates their population behavior and substantiate roles for ICAM-1, IL-2, and CTLA-4 in this process.

DISCUSSION

Based on the central role of T lymphocytes in host protection against pathogens and malignancies, mechanisms shaping antigen-specific T cell responses are studied extensively. Most studies focus on the impact of specialized regulatory cell types like mature DCs and Treg cells, which promote or curtail T cell responses, respectively. However, these studies do not reveal if individual $CD8^+$ T cells act entirely independent of each other or if their behavior is coordinated. We clarified this question by showing that T cell responses were concerted and that such regulation was not confined to specialized regulatory cell types like DCs or Treg cells. Instead, we provided evidence for an additional layer of regulation by showing that $CD8^+$ T cells themselves actively contributed to the regulation of their own population dynamics. Specifically, our work sketches a scenario in which activated T cells mutually promoted their expansion when only few of them were present but also limit further proliferation once sufficient numbers had been generated. This scenario is highly reminiscent of quorum-regulated systems, in which population members sense each other and adjust their behavior accordingly (Waters and Bassler, 2005). Such behavioral adaptation according to population density enables mutual promotion or inhibition of cellular expansion and differentiation, thereby conferring robustness to population responses. For T cell responses, achieving sufficient but preventing excessive expansion is important, because expanded T cell populations are crucial for pathogen elimination yet may also cause devastating immunopathology.

Quorum regulation requires communication among population members, which is facilitated by close proximity of cells. Activated T cells attract each other to their priming site (Hugues et al., 2007) and congregate into cell clusters by upregulating ICAM-1 and LFA-1 (Gérard et al., 2013; Zumwalde et al., 2013). We reasoned that these cell clusters constitute niches enabling T cells to communicate via soluble and

(H) Blood kinetics of 2×10^4 adoptively transferred GFP- versus *Icam1*-GFP-transgenic P14 T cells. Note that the different kinetics of P14 and P14 GFP cells in (D) and (H) are due to different numbers of transferred cells.

(I–O) Day 7 expansion and phenotype of endogenous $CD8^+$ T cells upon adoptive transfer of 2×10^4 GFP- versus *Icam1*-GFP-transgenic P14 T cells (I–K), of 2×10^4 GFP- versus *Il2*-GFP-transgenic P14 T cells (L,M) or of 1×10^5 GFP- versus *Ctla4*-GFP-transgenic P14 T cells (N and O).

Statistical tests: ANOVA (B and C), unpaired t test with Welch's correction (D, E, and G–O), and Mann-Whitney test (F). Data shown in this figure are representative of 2–3 independent experiments with 3 technical (A–C) or 3–5 (D–O) biological replicates each. Error bars depict mean ± SD. See also Figure S6.

membrane-bound receptor-ligand pairs. Supporting this notion, it is known that activated T cells can broadcast signals that modulate their behavior (Gérard et al., 2013; Polonsky et al., 2018; Sabatos et al., 2008; Zumwalde et al., 2013). However, it was unclear if this reflects a simple default program of T cell activation or if T cells actively modulate such signals. Our work provided evidence that activated T cells adjusted their communication to their population density. Furthermore, we identified a mechanism underlying this adjustment by revealing that T cell-expressed CD80 and CD86 fed two nested, antagonistic feedback circuits controling T cell behavior. This is possible because both CD80 and CD86 can bind to the receptors CD28 and CTLA-4, which confer stimulatory and inhibitory effects, respectively. Notably, while 60% of all cells expressing CD80 or CD86 in the spleen are T cells (Eberlein et al., 2012), the role of these molecules on T cells has largely been unresolved. Naive $CD8^+$ T cells express CD28, and some also express CD86. However, they do not cluster spontaneously, and bivalent ligand binding of CD28 requires concomitant TCR triggering (Sanchez-Lockhart et al., 2011), rendering it unlikely that this interaction mediates relevant communication among naive T cells. This situation changes once T cells recognize antigens presented by DCs, in which case TCR triggering licenses CD28 signaling mediated by APC-expressed CD80 and CD86. We showed that CD28 stimulation induced ICAM-1 and CD80 expression on T cells, which promoted clustering and mutual costimulation, respectively. An additional layer of complexity is added by the ability of T cells to trogocytose peptide-MHC complexes, CD80, and CD86 from APCs and present them on their surface (Huang et al., 1999; Hwang et al., 2000). This makes it difficult to distinguish the contributions of antigen presentation and costimulation by DCs and T cells within a cluster of T cells surrounding a DC. However, while within clusters, T cell- and DC-expressed CD80 and CD86 may act in concert, the relative contribution of T cell expressed molecules is expected to increase over time as activated T cells, but not DCs, rapidly proliferate. This expansion is supported by CD28-mediated expression of Bcl-xL and IL-2, which in turn induces Bcl-2. Our work revealed a crucial role for these anti-apoptotic molecules, because apoptosis effectively censored cell division already very early after activation. As IL-2 concentrations mirrored the density and abundance of activated T cells, cluster formation permits T cells to support their survival. Such population-intrinsic modulation of signal strength is a hallmark of quorum regulation. As CD28 and IL-2 also stimulate the expression of Myc (Heinzel et al., 2017), activated T cells are expected to also mutually promote their proliferation.

Quorum regulation frequently integrates feedback regulation, which we found in several instances: CD28 and IL-2 induced CD80 expression by activated T cells, which could in turn bind to CD28 to augment IL-2 production. This positive feedback loop acts to perpetuate T cell expansion. However, at some point T cell expansion needs to be limited in order to prevent immunopathology. This is accomplished by a negative feedback circuit acting via CTLA-4, which is also driven by CD28 and IL-2. CTLA-4 deprives CD28 of its ligands by competitive exclusion and also mediates inhibitory signals in *cis* (Contardi et al., 2005). Consistent with our observations, CTLA-4 has been reported to curtail IL-2 expression (Krummel and Allison, 1996; Walunas et al., 1996) and to promote apoptosis (Gribben et al., 1995; Scheipers and Reiser, 1998). Furthermore, we found that these antagonistic circuits differentially modulated ICAM-1 expression and T cell cluster stability. Both feedback circuits are connected by competition for CD80 and CD86. The outcome of this competition depends on the relative expression levels of CD28 and CTLA-4 at different points in time. CD28 was already present on naive T cells, whereas CTLA-4 expression lagged behind and depended on cell density. Thus, early after activation, CD28-driven T cell expansion dominates within clusters, whereas later and at high cell densities, CTLA-4 expression converts the initially activating interaction among T cells into an inhibitory one. We corroborated this scenario by constructing a dynamic mathematical model of the intertwined feedback loops fitted to the dynamics of interactome components. The model was purposely designed to be reductionist, as this allows the identification of crucial regulatory elements and avoids "overfitting" due to the use of too many parameters. The model showed that CD28 and IL-2R signaling, as well as the negative feedback provided by CTLA-4, is required to quantitatively explain T cell dynamics. The adaptive network architecture enables T cells to tune the relative activities of positive and negative feedback loops. Our model also confirmed the cell-densitiy dependence of this regulation. Additionaly, it indicated that the relative expression of IL-2 and CTLA-4 determines the transition from population expansion to contraction. Together, our results provide a mechanistic explanation how nested antagonistic feedback circuits homeostatically regulate T cell population dynamics across different cell counts and densities. Comparable results have been reported for a similar network engineered into yeast (Youk and Lim, 2014). Future model extensions incorporating spatiotemporal dynamics of cluster formation, cell migration, and IL-2 diffusion should broaden our understanding of quorum-regulation.

A recent landmark publication correlates cell density and IL-2 availability to CD4+ T cell behavior (Polonsky et al., 2018) but does not address how these factors are regulated. Our work on $CD8^+$ T cells corroborates and extends this concept by showing that T cells—vice versa—also actively modulate cell density and IL-2 abundance, and by delineating the mechanisms underlying such behavioral orchestration. While we did not investigate whether similar mechanisms also operate in CD4+ T cells, we consider this likely, because they express all relevant receptors and ligands involved in the nested feedback circuits we identified. Furthermore, IL-2 also modulates the expansion and differentiation of CD4+ T cells and promotes their expression of CTLA-4.

While our work provides a proof of concept demonstrating how a simple network of two nested antagonistic feedback circuits can regulate T cell population dynamics, it does not provide a comprehensive overview of all signals T cells could employ to mutually regulate their behavior. Other candidates predicted by our bioinformatic algorithm that could exert such functions are, for example, the interactions of FasL, PD-L1, IFNγ, TNFα, IL-18, or IL-1β with their receptors.

Furthermore, physiologically, T cell quorum regulation is embedded within substantially larger networks involving other cell types. Namely, CD80, CD86, and CTLA-4 are also highly expressed on DCs and Treg cells, respectively. We showed that

T cells also mutually regulated their population dynamics upon activation by DCs, exemplifying that T cell quorum regulation can integrate inputs derived from other cell types. The interplay of $CD8^+$ T cell population intrinsic and extrinsic regulatory mechanisms is important, because immune responses induced by different pathogens vary. Such external inputs will tune the balance of positive and negative feedback circuits of T cell quorum regulation upon different primary but also recall infections.

The interplay of T cell population extrinsic and intrinsic layers of regulation makes it challenging to investigate T cell-density-dependent regulation *in vivo*. To study this, in previous works titrated numbers of adoptively transferred TCR-transgenic T cells were activated *in vivo* (Polonsky et al., 2018). A downside of this approach is that increasing the numbers of transferred T cells promotes their competition for antigen and other extrinsic signals. These potential confounders make it difficult to attribute any differences observed solely to mutual regulation of activated T cells. We thus set out to more directly modulate T cell density *in vivo* by altering their ability to interact with each other. As ICAM-1 expression by T cells is dispensable for their priming by DCs but important for T cell clustering (Gérard et al., 2013; Zumwalde et al., 2013), we tracked adoptively transferred T cells lacking or overexpressing ICAM-1, which limits or promotes, respectively, their interaction with each other. Consistent with a role for clustering in promoting T cell survival, we found that $CD8^+$ T cell expansion scaled with their expression of ICAM-1. This was not a cell-intrinsic effect, as ICAM-1 overexpression also promoted the expansion of unmodified, endogenous $CD8^+$ T cells and directed their differentiation toward more KLRG-1 and less CD127 expression. These observations demonstrate that also *in vivo* $CD8^+$ T cells mutually regulate their expansion and differentiation. Mechanistically, the effects observed are consistent with increased exposure to IL-2 upon T cell clustering, because IL-2 increases T cell expansion and KLRG-1 expression and decreases CD127 expression (Pipkin et al., 2010). Our mathematical model predicted that within clusters the relative expression levels of IL-2 and CTLA-4 determine T cell population dynamics, underscoring a functional antagonism of both molecules. Accordingly, we observed that while expression of IL-2 by transferred cells mimicked the effect of ICAM-1 overexpression on expansion and differentiation of endogenous $CD8^+$ T cells, transfer of *Ctla4* transgenic T cells had an opposite effect. $CD8^+$ T cell expression patterns of KLRG-1 and CD127 are widely used to define their differentiation into effector and memory precursor cells. In this regard, the effects we observed on the expression of KLRG-1 and CD127 when we modulated elements of the T cell quorum regulation network *in vivo* could suggest that T cell quorum regulation also modulates the balance between effector and memory $CD8^+$ T cell differentiation. While we did not investigate this topic in our current work, a correlation between cell density and CD4+ T cell differentiation has been described (Polonsky et al., 2018).

In summary, our work showcases how communication among activated $CD8^+$ T cells enables collective behavioral regulation. Thus, rather than constituting a population of individualists, activated T lymphocytes function in a cooperative manner. While our *in vivo* and *in vitro* observations are well in line with each other, the experiments are based on perturbation of the regulatory networks. Thus, they do not directly test to which degree physiological variation of the signals modulates T cell behavior. This would require the development of experimental setups that link quantitative information on the amount and/or intensity of interactions a specific T cell experiences *in vivo* to the fate of its progeny—an important aim for future research. Dissecting the mechanisms underlying T cell social behavior helps to understand how robustness is conferred to immune responses. Furthermore, exploiting these mechanisms should improve the efficacy of immunotherapies in different diseases like cancer, infections, and immunodeficiencies.

STAR★METHODS

Detailed methods are provided in the online version of this paper and include the following:

- KEY RESOURCES TABLE
- LEAD CONTACT AND MATERIALS AVAILABILITY
- EXPERIMENTAL MODEL AND SUBJECT DETAILS
  - Mice
  - Cell culture
- METHOD DETAILS
  - Plasmids
  - Cell culture
  - Retroviral transduction
  - Adoptive transfer & infections
  - Flow cytometry
  - Time-lapse imaging
  - Confocal imaging of T cell clusters
  - Receptor-ligand pair prediction for T cells
  - Mathematical model
- QUANTIFICATION AND STATISTICAL ANALYSIS
- DATA AND CODE AVAILABILITY

SUPPLEMENTAL INFORMATION

Supplemental Information can be found online at https://doi.org/10.1016/j.immuni.2020.01.018.

ACKNOWLEDGMENTS

We acknowledge Susanne Kirschnek and Susanne Heinzel for providing plasmids, Jürgen Brandel for support on video compilation, and Clara Kamüller and Caro Schuler for mouse husbandry. We are grateful to Hanspeter Pircher and Peter Aichele for discussions, as well as Monika Wolkers, Susanne Heinzel, Carmen Gerlach, and Jannie Borst for critically reading the manuscript. Work in the authors' labs was supported by the Netherlands Organization for Scientific Research (NWO; grant 864.12.013 to J.B.B.), an International Junior Research Group grant (N-LW-2016-370) from the Elite Network of Bavaria, Bavarian State Ministry of Science and the Arts (to J.P.B.), and funding from Technical University of Munich (to J.P.B.) and the German Research Foundation (DFG) (to J.P.B. and J.C.R.: grant no. RO 4120/2-1) and the SFB1160 (project number 15 to J.C.R.).

AUTHOR CONTRIBUTIONS

Conceptualization, J.C.R.; Methodology, J.C.R., S.Z., M.M.P., J.B.B., J.P.B., A.G., T.L., A. Gavrilov, A. Gerard, and T.N.S.; Mathematical Modeling, M.M.P., J.B.B.; Investigation, S.Z., M.M.P., J.B.B., P.M., J.P.B., J.B., A. Gavrilov, and J.C.R.; Writing—Original Draft, J.C.R.; Writing—Review & Editing, M.M.P., J.B.B., N.B., T.S., and J.C.R.; Funding Acquisition, J.B.B., J.P.B., and J.C.R.; Resources, N.B., S.E., T.L., A.G., and T.S.; Supervision, J.C.R. and J.B.B.

DECLARATION OF INTERESTS

The authors declare no competing interests.

Received: April 20, 2019
Revised: September 22, 2019
Accepted: January 24, 2020
Published: February 11, 2020

REFERENCES

Azuma, M., Yssel, H., Phillips, J.H., Spits, H., and Lanier, L.L. (1993). Functional expression of B7/BB1 on activated T lymphocytes. J. Exp. Med. *177*, 845–850.

Ben-Shlomo, I., Yu Hsu, S., Rauch, R., Kowalski, H.W., and Hsueh, A.J. (2003). Signaling receptome: a genomic and evolutionary perspective of plasma membrane receptors involved in signal transduction. Sci. STKE *2003*, RE9.

Bosch, A.J.T., Bolinger, B., Keck, S., Stepanek, O., Ozga, A.J., Galati-Fournier, V., Stein, J.V., and Palmer, E. (2017). A minimum number of autoimmune T cells to induce autoimmunity? Cell. Immunol. *316*, 21–31.

Bretscher, P.A. (1999). A two-step, two-signal model for the primary activation of precursor helper T cells. Proc. Natl. Acad. Sci. USA *96*, 185–190.

Buchholz, V.R., Flossdorf, M., Hensel, I., Kretschmer, L., Weissbrich, B., Gräf, P., Verschoor, A., Schiemann, M., Höfer, T., and Busch, D.H. (2013). Disparate individual fates compose robust CD8+ T cell immunity. Science *340*, 630–635.

Castelló-Cros, R., and Cukierman, E. (2009). Stromagenesis during tumorigenesis: characterization of tumor-associated fibroblasts and stroma-derived 3D matrices. Methods Mol. Biol. *522*, 275–305.

Chen, S., Harrigan, P., Heineike, B., Stewart-Ornstein, J., and El-Samad, H. (2013). Building robust functionality in synthetic circuits using engineered feedback regulation. Curr. Opin. Biotechnol. *24*, 790–796.

Contardi, E., Palmisano, G.L., Tazzari, P.L., Martelli, A.M., Falà, F., Fabbi, M., Kato, T., Lucarelli, E., Donati, D., Polito, L., et al. (2005). CTLA-4 is constitutively expressed on tumor cells and can trigger apoptosis upon ligand interaction. Int. J. Cancer *117*, 538–550.

Dennehy, K.M., Elias, F., Zeder-Lutz, G., Ding, X., Altschuh, D., Lühder, F., and Hünig, T. (2006). Cutting edge: monovalency of CD28 maintains the antigen dependence of T cell costimulatory responses. J. Immunol. *176*, 5725–5729.

Eberlein, J., Davenport, B., Nguyen, T.T., Victorino, F., Sparwasser, T., and Homann, D. (2012). Multiple layers of CD80/86-dependent costimulatory activity regulate primary, memory, and secondary lymphocytic choriomeningitis virus-specific T cell immunity. J. Virol. *86*, 1955–1970.

Fritsch, F.N., and Carlson, R.E. (1980). Monotone piecewise cubic interpolation. SIAM J. Numer. Anal. *17*, 238–246.

Gérard, A., Khan, O., Beemiller, P., Oswald, E., Hu, J., Matloubian, M., and Krummel, M.F. (2013). Secondary T cell-T cell synaptic interactions drive the differentiation of protective CD8+ T cells. Nat. Immunol. *14*, 356–363.

Gerlach, C., Rohr, J.C., Perié, L., van Rooij, N., van Heijst, J.W., Velds, A., Urbanus, J., Naik, S.H., Jacobs, H., Beltman, J.B., et al. (2013). Heterogeneous differentiation patterns of individual CD8+ T cells. Science *340*, 635–639.

Graeber, T.G., and Eisenberg, D. (2001). Bioinformatic identification of potential autocrine signaling loops in cancers from gene expression profiles. Nat. Genet. *29*, 295–300.

Gribben, J.G., Freeman, G.J., Boussiotis, V.A., Rennert, P., Jellis, C.L., Greenfield, E., Barber, M., Restivo, V.A., Jr., Ke, X., Gray, G.S., et al. (1995). CTLA4 mediates antigen-specific apoptosis of human T cells. Proc. Natl. Acad. Sci. USA *92*, 811–815.

Heinzel, S., Binh Giang, T., Kan, A., Marchingo, J.M., Lye, B.K., Corcoran, L.M., and Hodgkin, P.D. (2017). A Myc-dependent division timer complements a cell-death timer to regulate T cell and B cell responses. Nat. Immunol. *18*, 96–103.

Hommel, M., and Kyewski, B. (2003). Dynamic changes during the immune response in T cell-antigen-presenting cell clusters isolated from lymph nodes. J. Exp. Med. *197*, 269–280.

Huang, J.F., Yang, Y., Sepulveda, H., Shi, W., Hwang, I., Peterson, P.A., Jackson, M.R., Sprent, J., and Cai, Z. (1999). TCR-Mediated internalization of peptide-MHC complexes acquired by T cells. Science *286*, 952–954.

Hudrisier, D., Riond, J., Mazarguil, H., Gairin, J.E., and Joly, E. (2001). Cutting edge: CTLs rapidly capture membrane fragments from target cells in a TCR signaling-dependent manner. J. Immunol. *166*, 3645–3649.

Hugues, S., Scholer, A., Boissonnas, A., Nussbaum, A., Combadière, C., Amigorena, S., and Fetler, L. (2007). Dynamic imaging of chemokine-dependent CD8+ T cell help for CD8+ T cell responses. Nat. Immunol. *8*, 921–930.

Hwang, I., Huang, J.F., Kishimoto, H., Brunmark, A., Peterson, P.A., Jackson, M.R., Surh, C.D., Cai, Z., and Sprent, J. (2000). T cells can use either T cell receptor or CD28 receptors to absorb and internalize cell surface molecules derived from antigen-presenting cells. J. Exp. Med. *191*, 1137–1148.

Jones, E., Oliphant, T.E., Peterson, P. SciPy 1.0 Contributors, (2001). SciPy: Open source scientific tools for Python. http://www.scipy.org/.

Khanna, K.M., McNamara, J.T., and Lefrançois, L. (2007). In situ imaging of the endogenous CD8 T cell response to infection. Science *318*, 116–120.

Kitamura, T., Koshino, Y., Shibata, F., Oki, T., Nakajima, H., Nosaka, T., and Kumagai, H. (2003). Retrovirus-mediated gene transfer and expression cloning: powerful tools in functional genomics. Exp. Hematol. *31*, 1007–1014.

Klebanoff, C.A., Scott, C.D., Leonardi, A.J., Yamamoto, T.N., Cruz, A.C., Ouyang, C., Ramaswamy, M., Roychoudhuri, R., Ji, Y., Eil, R.L., et al. (2016). Memory T cell-driven differentiation of naive cells impairs adoptive immunotherapy. J. Clin. Invest. *126*, 318–334.

Krummel, M.F., and Allison, J.P. (1996). CTLA-4 engagement inhibits IL-2 accumulation and cell cycle progression upon activation of resting T cells. J. Exp. Med. *183*, 2533–2540.

Kyburz, D., Aichele, P., Speiser, D.E., Hengartner, H., Zinkernagel, R.M., and Pircher, H. (1993). T cell immunity after a viral infection versus T cell tolerance induced by soluble viral peptides. Eur. J. Immunol. *23*, 1956–1962.

Li, K.P., Shanmuganad, S., Carroll, K., Katz, J.D., Jordan, M.B., and Hildeman, D.A. (2017). Dying to protect: cell death and the control of T-cell homeostasis. Immunol. Rev. *277*, 21–43.

Lindstein, T., June, C.H., Ledbetter, J.A., Stella, G., and Thompson, C.B. (1989). Regulation of lymphokine messenger RNA stability by a surface-mediated T cell activation pathway. Science *244*, 339–343.

McKay, M.D., Beckman, R.J., and Conover, W.J. (1979). A Comparison of Three Methods for Selecting Values of Input Variables in the Analysis of Output from a Computer Code. Technometrics *21*, 239–245.

Mempel, T.R., Henrickson, S.E., and Von Andrian, U.H. (2004). T-cell priming by dendritic cells in lymph nodes occurs in three distinct phases. Nature *427*, 154–159.

Miller, M.J., Safrina, O., Parker, I., and Cahalan, M.D. (2004). Imaging the single cell dynamics of CD4+ T cell activation by dendritic cells in lymph nodes. J. Exp. Med. *200*, 847–856.

Pawson, A.J., Sharman, J.L., Benson, H.E., Faccenda, E., Alexander, S.P., Buneman, O.P., Davenport, A.P., McGrath, J.C., Peters, J.A., Southan, C., et al.; NC-IUPHAR (2014). The IUPHAR/BPS Guide to PHARMACOLOGY: an expert-driven knowledgebase of drug targets and their ligands. Nucleic Acids Res. *42*, D1098–D1106.

Peach, R.J., Bajorath, J., Naemura, J., Leytze, G., Greene, J., Aruffo, A., and Linsley, P.S. (1995). Both extracellular immunoglobin-like domains of CD80 contain residues critical for binding T cell surface receptors CTLA-4 and CD28. J. Biol. Chem. *270*, 21181–21187.

Pipkin, M.E., Sacks, J.A., Cruz-Guilloty, F., Lichtenheld, M.G., Bevan, M.J., and Rao, A. (2010). Interleukin-2 and inflammation induce distinct transcriptional programs that promote the differentiation of effector cytolytic T cells. Immunity *32*, 79–90.

Pletinckx, K., Vaeth, M., Schneider, T., Beyersdorf, N., Hünig, T., Berberich-Siebelt, F., and Lutz, M.B. (2015). Immature dendritic cells convert anergic nonregulatory T cells into Foxp3- IL-10+ regulatory T cells by engaging CD28 and CTLA-4. Eur. J. Immunol. *45*, 480–491.

Polonsky, M., Rimer, J., Kern-Perets, A., Zaretsky, I., Miller, S., Bornstein, C., David, E., Kopelman, N.M., Stelzer, G., Porat, Z., et al. (2018). Induction of CD4 T cell memory by local cellular collectivity. Science *360*.

Prabhu Das, M.R., Zamvil, S.S., Borriello, F., Weiner, H.L., Sharpe, A.H., and Kuchroo, V.K. (1995). Reciprocal expression of co-stimulatory molecules, B7-1 and B7-2, on murine T cells following activation. Eur. J. Immunol. *25*, 207–211.

Sabatos, C.A., Doh, J., Chakravarti, S., Friedman, R.S., Pandurangi, P.G., Tooley, A.J., and Krummel, M.F. (2008). A synaptic basis for paracrine interleukin-2 signaling during homotypic T cell interaction. Immunity *29*, 238–248.

Sanchez-Lockhart, M., Kim, M., and Miller, J. (2011). Cutting edge: A role for inside-out signaling in TCR regulation of CD28 ligand binding. J. Immunol. *187*, 5515–5519.

Scheipers, P., and Reiser, H. (1998). Fas-independent death of activated CD4(+) T lymphocytes induced by CTLA-4 crosslinking. Proc. Natl. Acad. Sci. USA *95*, 10083–10088.

Thompson, C.B., Lindsten, T., Ledbetter, J.A., Kunkel, S.L., Young, H.A., Emerson, S.G., Leiden, J.M., and June, C.H. (1989). CD28 activation pathway regulates the production of multiple T-cell-derived lymphokines/cytokines. Proc. Natl. Acad. Sci. USA *86*, 1333–1337.

Voisinne, G., Nixon, B.G., Melbinger, A., Gasteiger, G., Vergassola, M., and Altan-Bonnet, G. (2015). T Cells Integrate Local and Global Cues to Discriminate between Structurally Similar Antigens. Cell Rep. *11*, 1208–1219.

Walunas, T.L., Bakker, C.Y., and Bluestone, J.A. (1996). CTLA-4 ligation blocks CD28-dependent T cell activation. J. Exp. Med. *183*, 2541–2550.

Waters, C.M., and Bassler, B.L. (2005). Quorum sensing: cell-to-cell communication in bacteria. Annu. Rev. Cell Dev. Biol. *21*, 319–346.

Wu, Y., Guo, Y., Huang, A., Zheng, P., and Liu, Y. (1997). CTLA-4-B7 interaction is sufficient to costimulate T cell clonal expansion. J. Exp. Med. *185*, 1327–1335.

Yoon, H., Kim, T.S., and Braciale, T.J. (2010). The cell cycle time of CD8+ T cells responding in vivo is controlled by the type of antigenic stimulus. PLoS ONE *5*, e15423.

You, L., Cox, R.S., 3rd, Weiss, R., and Arnold, F.H. (2004). Programmed population control by cell-cell communication and regulated killing. Nature *428*, 868–871.

Youk, H., and Lim, W.A. (2014). Secreting and sensing the same molecule allows cells to achieve versatile social behaviors. Science *343*, 1242782.

Zumwalde, N.A., Domae, E., Mescher, M.F., and Shimizu, Y. (2013). ICAM-1-dependent homotypic aggregates regulate CD8 T cell effector function and differentiation during T cell activation. J. Immunol. *191*, 3681–3693.

STAR★METHODS

KEY RESOURCES TABLE

REAGENT or RESOURCE	SOURCE	IDENTIFIER
Antibodies		
Anti-Mouse/Rat CD90.1 (Thy1.1) FITC (clone OX-7)	BD Bioscience	Cat#561973, RRID: AB_10898011
Anti-Mouse Ki67 PerCP-Cy5.5 (clone B56)	BD Bioscience	Cat#561284, RRID: AB_10611574
Anti-Mouse CD8a Brilliant Violet 510 (clone 53-6.7)	BioLegend,	Cat#100752, RRID: AB_2563057
Anti-Mouse CD45.1 Alexa Fluor 700 (clone A20)	BioLegend	Cat#110723, RRID: AB_493732
Anti-Mouse CD45.2 PE/Cy7 (clone 104)	BioLegend	Cat#09830, RRID: AB_1186098
Anti-Mouse CD45.2 Alexa Fluor (clone 104)	BioLegend	Cat#109821, RRID: AB_493730
Anti-Mouse/Rat CD90.1 (Thy-1.1) PE/Cy7 (clone OX-7)	BioLegend	Cat#202518, RRID: AB_1659223
Anti-Mouse CD90.2 (Thy-1.2) Alexa Fluor 700 (clone 30-H12)	BioLegend	Cat#105320, RRID: AB_493725
Anti-Mouse CD80 PE/Cy7 (clone 16-10A1)	BioLegend	Cat#104734, RRID: AB_2563113
Anti-Mouse CD80 Brilliant Violet 421™ (clone 16-10A1)	BioLegend	Cat#104726, RRID: AB_2561445
Anti-Mouse CD86 APC (clone GL-1)	BioLegend	Cat#105012, RRID: AB_493342
Anti-Mouse Bcl-2 PE/Cy7 (clone BCL/10C4)	BioLegend	Cat#633511, RRID: AB_2565246
Anti-Mouse CD11a LEAF™ Purified (clone M17/4)	BioLegend	Cat#101110, RRID: AB_312783
Anti-Mouse CD54 (ICAM-1) APC (clone YN1/1.7.4)	BioLegend	Cat#116120, RRID: AB_10612936
Anti-Mouse CD152 (CTLA-4) PE (clone UC10-4B9)	BioLegend	Cat#106306, RRID: AB_313255
Anti-Mouse CD152 (CTLA-4) APC (clone UC10-4B9)	BioLegend	Cat#106310, RRID: AB_2087653
Anti-Mouse CD152 (CTLA-4) Biotin (clone UC10-4B9)	BioLegend	Cat#106303, RRID: AB_313252
Anti-mouse CD25 BV875 (clone PC61)	BioLegend	Cat# 102051, RRID: AB_2564131
Anti-Mouse CD28 LEAF Purified (clone 37.51)	BioLegend	Cat#102112, RRID: AB_312877
Anti-Mouse CD127 (IL-7Rα) PE (clone A7R34)	BioLegend	Cat#135010, RRID: AB_1937251
Anti-Mouse CD127 BV421 (clone A7R34)	BioLegend	Cat#135023, RRID: AB_10897948
Anti-Mouse Bcl-xL Alexa Fluor 647 (clone 54H6)	Cell Signaling Technology	Cat#86387S, RRID: AB_2800078
Anti-Mouse CD8a PerCP-eFluor 710 (clone 53-6.7)	Thermo Fisher Scientific	Cat#46-0081-80, RRID: AB_1834434
Anti-Mouse CD8a FITC (clone 53-6.7)	Thermo Fisher Scientific	Cat#11-0081-85, RRID: AB_464916
Anti-Mouse CD45.1 PerCP-Cyanine5.5 (clone A20)	Thermo Fisher Scientific	Cat#45-0453-80, RRID: AB_925750
Anti-Mouse CD90.2 (Thy-1.2) APC (clone 53-2.1)	Thermo Fisher Scientific	Cat#17-0902-82, RRID: AB_469422
Anti-Mouse CD11a (LFA-1alpha) PE (clone M17/4)	Thermo Fisher Scientific	Cat#12-0111-82, RRID: AB_465544
Anti-Mouse KLRG-1 PerCP-eFluor710 (clone 2F1)	Thermo Fisher Scientific	Cat#46-5893-82, RRID: AB_10670282
Anti-Mouse KLRG-1 APC (clone 2F1)	Thermo Fisher Scientific	Cat#17-5893-82, RRID: AB_469469
Anti-Mouse CD28 fab fragments generated from a-CD28 mAb (clone E18)	Dennehy et al., 2006	N/A
Anti-Mouse CTLA-4 (clone UC10-4F10)	BioXCell	Cat#BE0032, RRID: AB_1107598
Anti-Mouse IL-2 *InVivo*mAb (clone S4B6-1)	BioXCell	Cat# BE0043-1, RRID: AB_1107705
Anti-Mouse IL-2 *InVivo*mAb (clone JES6-1A12)	BioXCell	Cat#BE0043, RRID: AB_1107702
Anit-Mouse Interferon-γ *InVivo*mAb (clone XMG1.2)	BioXCell	Cat# BE0055, RRID: AB_1107694
Bacterial and Virus Strains		
One Shot™ TOP10 Chemically Competent *E. coli*	Thermo Fisher Scientific	Cat#C404010
LCMV-WE	H. Pircher (Freiburg, Germany)	N/A

(*Continued on next page*)

Continued

REAGENT or RESOURCE	SOURCE	IDENTIFIER
Chemicals, Peptides, and Recombinant Proteins		
Alexa Fluor 488 Streptavidin	BioLegend	Cat#405235
Precision Count Beads	BioLegend	Cat#424902
CellTrace Violet Cell Proliferation Kit	Thermo Fisher Scientific	Cat#C34557
eBioscience CFSE	Thermo Fisher Scientific	Cat#65-0850-84
LIVE/DEAD Fixable Near-IR Dead Cell Stain Kit	Thermo Fisher Scientific	Cat#L10119
Zombie Violet Fixable Viability Kit	BioLegend	Cat#423113
Phorbol 12-myristate 13-acetate (PMA)	Sigma-Aldrich	Cat#P8139, CAS: 16561-29-8
Ionomycin	Sigma-Aldrich	Cat#407952, CAS: 56092-82-1
Concanavalin A (ConA)	Sigma-Aldrich	Cat# C5275, CAS: 11028-71-0
Recombinant Human IL-2 (Proleukin S)	Novartis Pharma GmbH	Cat#A2542
Recombinant murine IL-7	PeproTech	Cat#217-17
Recombinant murine GM-CSF	PeproTech	Cat#3150320
Recombinant murine IFN-γ	PeproTech	Cat#315-05
Lipopolysaccharides (LPS)	Sigma-Aldrich	Cat#L3024
LCMV gp33 epitope (amino acid sequence: KAVYNFATC)	PolyPeptide	N/A
FuGENE 6 Transfection Reagent	Promega	Cat#E2691
Iscove's Modified Dulbecco's Medium (IMDM) + L-Glutamine	Thermo Fisher Scientific	Cat#21980065
Penicillin-Streptomycin 5,000 U/mL (P/S)	Thermo Fisher Scientific	Cat#15070063
Fetal Bovine Serum	PAN Biotech	Cat#P30-1502, Lot#P150718
β-Mercaptoethanol	AppliChem	Cat#A1108, CAS: 60-24-2
RetroNectin Recombinant Human Fibronectin Fragment	Takara	Cat#T100A
DAPI	Sigma-Aldrich	Cat#D9542, CAS: 28718-90-3
Fluoromount-G	SouthernBiotech	Cat#0100-01
Lysing Solution 10X Concentrate	BD Bioscience	Cat#349202
Bovine Serum Albumin	Roche	Cat#10735086001
Puromycin	Applichem	Cat#A2856
Blasticidin S	Applichem	Cat#A3784
Poly-L-ornithine hydrobromide	Sigma-Aldrich	Cat#3655, CAS: 27378-49-0
Critical Commercial Assays		
Mouse IL-2 ELISA MAX Deluxe	BioLegend	Cat#431006
eBioscience Foxp3 / Transcription Factor Staining Buffer Set	Thermo Fisher Scientific	Cat#00-5523-00
Mouse CD8 T Lymphocyte Enrichment Set - DM	BD Bioscience	Cat#558471
NEBuilder HiFi DNA Assembly Master Mix	New England BioLabs	Cat#E2621L
Experimental Models: Cell Lines		
Human: Platinum-E retroviral packaging cell line	Cell Biolabs	Cat#RV-101, RRID:CVCL_B488
Experimental Models: Organisms/Strains		
Mouse: B6;D2-Tg(TcrLCMV)318Sdz/JDvsJ	H. Pircher	N/A
Mouse: B6.129S4-*Cd80*^{tm1Shr} *Cd86*^{tm2Shr}/J	The Jackson Laboratory	Stock No: 003610, RRID: IMSR_JAX:003610
Mouse: C57BL/6	Janvier Labs	Cat#SC-C57N-F
Mouse: B6.SJL-Ptprc^{a}Pepc^{b}/BoyJ	The Jackson Laboratory	Stock No: 002014, RRID:IMSR_JAX:002014
Mouse: B6.129(Cg)-*Gt(ROSA)26Sor*$^{tm4(ACTB-tdTomato,-EGFP)Luo}$/J	The Jackson Laboratory	Stock No: 007676, RRID:IMSR_JAX:007676
Mouse: B6.129S4-*Icam1*^{tm1Jcgr}/J	The Jackson Laboratory	Stock No: 002867, RRID:IMSR_JAX:002867

(*Continued on next page*)

Continued

REAGENT or RESOURCE	SOURCE	IDENTIFIER
Recombinant DNA		
Plasmid: pMx-Cd80-IRES-GFP	This manuscript	N/A
Plasmid: pMx-Cd80Y201A-IRES-GFP	This manuscript	N/A
Plasmid: pMx-Cd86-IRES-GFP	This manuscript	N/A
Plasmid: pMx-Cd86Q35A-IRES-GFP	This manuscript	N/A
Plasmid: pMx-Ctla-4-IRES-GFP	This manuscript	N/A
Plasmid: pMx-Cd25-IRES-GFP	This manuscript	N/A
Plasmid: pMx-Il-2-IRES-GFP	This manuscript	N/A
Plasmid: pMx-Icam-1-IRES-GFP	This manuscript	N/A
Plasmid: pMx-Bcl-2-IRES-GFP	This manuscript	N/A
Plasmid: pMx-Bcl-xL-IRES-GFP	This manuscript	N/A
Plasmid: pMx-myc	Heinzel et al., 2017	N/A
Plasmid: pMx-IRES-GFP	Kitamura et al., 2003	N/A
Software and Algorithms		
Prism8 (v8.1.0)	GraphPad Software	https://www.graphpad.com/
FlowJo X (v10.0.7r2 and v10.2)	BD Bioscience	https://www.flowjo.com/
Inkscape (v0.92)	The Inkscape project	https://inkscape.org
Code predicting candidate receptor-ligands pairs	This manuscript	N/A
Mathematical modeling of T cell dynamics	This manuscript	N/A
Other		
Database of ligand-receptor partners (DLRP)	Graeber and Eisenberg, 2001	http://dip.doe-mbi.ucla.edu/dip/DLRP.cgi
human plasma membrane receptome (HPMR)	Ben-Shlomo et al., 2003	http://www.receptome.org/
IUPHAR database	Pawson et al., 2014	http://www.guidetopharmacology.org/linking.jsp
CD8 T cell gene expression data LCMV	https://www.ncbi.nlm.nih.gov/geo/	GEO: GSE30431
CD8 T cell gene expression data *Listeria monocytogenes* and VSV	https://www.ncbi.nlm.nih.gov/geo/	GEO: GSE15907

LEAD CONTACT AND MATERIALS AVAILABILITY

Further information and requests for resources and reagents should be directed to and will be fulfilled by the Lead Contact, Jan C. Rohr (jan.rohr@uniklinik-freiburg.de)

EXPERIMENTAL MODEL AND SUBJECT DETAILS

Mice

Animal experiments were approved by local governmental authorities (Regierungspräsidium Freiburg) and performed in accordance with EU guidelines. P14 TCR transgenic mice (TcrLCMV)318Sdz/JDvsJ) were originally described and provided by H. Pircher (Kyburz et al., 1993). *Cd80*$^{-/-}$*Cd86*$^{-/-}$ (B6.129S4-*Cd80*^{tm1Shr} *Cd86*^{tm2Shr}/J), *Cd45.1*$^{+/+}$ (B6.SJL-Ptprc^{a}Pepc^{b}/BoyJ), *Icam1*$^{-/-}$ (B6.129S4-*Icam1*^{tm1Jcgr}/J) and mTmG (B6.129(Cg)-*Gt(ROSA)26Sor*$^{tm4(ACTB-tdTomato,-EGFP)Luo}$/J) mice were from The Jackson Laboratory. C57BL/6 mice were from Janvier Labs. To generate TCR-transgenic *Cd80*$^{-/-}$*Cd86*$^{-/-}$, *Cd45.1*$^{+/+}$, mTmG or *Icam1*$^{-/-}$ animals, P14 mice were crossed with the respective strains. All mice had previously been backcrossed to a C57BL/6 background for ten generations. For all *in vivo* cell transfer studies sex-matched 8-12 week old C57BL/6 recipient mice were used. Male and female mice were used for experiments with no differences observed within the parameters analyzed. Mice were housed under specific pathogen-free conditions in groups of up to five mice

Cell culture

Primary cells and cell lines were cultured at 37°C, 5% CO_2 in a humidified environment. Primary cells of 6-26 week old male and female mice were used, which were sex-matched in co-culture experiments. Platinum-E cells were cultured in presence of drug selection (10 μg/mL blasticidin, 1 μg/mL puromycin, both Applichem).

METHOD DETAILS

Plasmids

DNA fragments encoding murine *Cd80*, *Cd86*, *Cd28*, *Ctla4*, *Cd25*, *Il2* and *Icam1* were either generated from splenocyte cDNA or ordered as gblocks (Integrated DNA Technologies). Template plasmids encoding murine *Bcl-2* and *Bcl-xL* cDNAs were generously provided by Susanne Kirschneck. Side-directed mutagenesis was performed by overlap PCR using primers containing the desired mutations. DNA fragments were cloned into retroviral pMx-vectors (Kitamura et al., 2003) using NEBuilder® HiFi DNA Assembly reagents (New England Biolabs). The pMx-myc plasmid (Heinzel et al., 2017) was a kind gift from Susanne Heinzel. All transgenes were sequence-verified prior to use.

Cell culture

Cells were cultured in IMDM L-Glutamin, PenStrep (both from Thermo Fisher Scientific), 10% FCS (PAN Biotech), 5mM β-Mercaptoethanol (Applichem), in 96-well u-, v- or flat-bottom plates (Greiner). Dendritic cells were generated by culturing murine bone marrow cells in GM-CSF (20 ng/mL, Peprotech) for 5 days and matured by addition of LPS (50ng/mL, Sigma-Aldrich) for 16 h. Mature DCs were pulsed with 10^{-6} M of LCMV gp33-epitope (amino acid sequence: KAVYNFATC) (PolyPeptide) for 1 h at 37°C. $CD8^+$ T cells were magnetically purified from spleens and/or lymph nodes (Mouse CD8 T lymphocyte enrichment set – DM, BD Biosciences). In some experiments enriched $CD8^+$ T cells were labeled with 1-10 μM CFSE or CTV proliferation dyes (Thermo Fisher Scientific). Unless stated otherwise, $CD8^+$ T cells were activated by adding either 10^{-7} M gp33 peptide or 10^4 peptide pulsed DCs. Interleukin-2 (Proleukin, Novartis) was used at 20 ng/mL unless stated otherwise. Interferon-γ (PeproTech) was used at 100 ng/mL The following unconjugated antibodies were used: anti-CD28 (37.51) at 1 μg/mL (BioLegend), anti-CTLA-4 (UC10-4F10) (BioXcell) at 10 μg/mL, anti-LFA-1 (M17/4) (BioLegend) at 20 μg/mL, anti-IFN-γ (XMG1.2) (BioXcell) at 10 μg/mL. CD28 antibody Fab-fragments were generated as described (Pletinckx et al., 2015). Briefly, anti-CD28 mAb (clone E18) (Dennehy et al., 2006) were concentrated and digested using immobilized papain under continuous mixing for 5 h at 37°C, followed by Protein A-purification. CD28-Fab fragments were used at 10 μg/mL. Anti-IL-2 antibodies clones S4B6 and JES6 (BioXcell) were used simultaneously at 5 μg/mL each. IL-2 concentrations in cell culture supernatants were determined using the mouse IL-2 ELISA MAX Kit (BioLegend).

Retroviral transduction

Replication-deficient retrovirus was generated by plasmid transfection of platinum-e packaging cells using Fugene 6 (Promega). Retrovirus-containing supernatant was harvested after 24- and/or 48 h and immediately used for transductions by spin-infection (90 min. 2,000 rpm, 30°C). Transductions were performed in non-tissue-culture treated 24-wells plates that had been coated with retronectin (20 μg/mL, TaKaRa) overnight and blocked with 2% BSA (Roche) for 1/2 h. Total splenocytes or purified $CD8^+$ T cells were activated 24 h prior to transduction by either cognate peptide, ConA (2 μg/mL, Sigma-Aldrich) + murine IL-7 (1 ng/mL, Peprotech), or 50 ng/mL PMA + 0.5 μg/mL Ionomycin (both Sigma-Aldrich). Transduction efficiencies ranged from 30%–80% as determined by flow cytometry.

Adoptive transfer & infections

Unless stated otherwise mice were adoptively transferred with 10^3 purified $CD8^+$ P14 T cells intravenously. For transfer of retrovirally transduced cells, total splenocytes were harvested 4 h post spin infection and were assessed for frequency of $CD8^+$ T cells. $2x10^4$-$1x10^5$ $CD8^+$ T cells were transferred intravenously. Mice were infected with 200 PFU LCMV WE intravenously. The LCMV strain WE was kindly provided by H. Pircher. Blood lymphocytes were analyzed after hypotonic erythrocyte lysis (BD FACS Lysing Solution, BD Biosciences). Spleens and lymph nodes were dissected using 70 μm cell strainers (Greiner).

Flow cytometry

The following fluorescent dye-conjugated antibodies were used: anti-CD90.1 (OX-7), anti-Ki67 (B56) (BD Bioscience); anti-CD8 (53-6.7), anti-CD45.1 (A20), anti-CD45.2 (104), anti-CD90.1 (OX-7), anti-CD90.2 (30-H12), anti-CD80 (16-10A1), anti-CD86 (GL-1), anti-Bcl-2 (BCL/10C4), anti-CD54 (YN1/1.7.4), anti-CD152 (UC10-4B9), anti-CD25 (PC61), anti-CD127 (A7R34) (BioLegend); anti-Bcl-xL (54H6) (Cell Signaling Technology); anti-CD8 (53-6.7), anti-CD45.1 (A20), anti-CD90.2 (53-2.1), anti-CD11a (M17/4), anti-KLRG-1 (2F1) (Thermo Fisher Scientific). For intracellular staining, cells were fixed and permeabilized using the FoxP3 transcription factor staining buffer set (Thermo Fisher Scientific). For cell quantification, precision count beads (BioLegend) were added to wells prior to cell harvest. CTLA-4 was stained for 30 min at 37°C, whereas all other antigens were stained at 4°C. Live/dead viability dyes were from Thermo Fisher Scientific and BioLegend. Cells were analyzed on a BD Fortessa flow cytometer (BD Bioscience). All FACS-analyses were performed on gated $CD8^+$ live cells.

Time-lapse imaging

For imaging of T cell clustering gp33-stimulated, purified 10^5 $CD8^+$ T cells from tdTomato-transgenic (mTmG) P14 mice were seeded in 0.01% Poly-L-ornithine (Sigma-Aldrich) coated 96-well flat-bottom plates and incubated in an Incucyte S3 live-cell analysis system (Essen BioScience). Per well 4 brightfield and fluorescent images were taken every 2 h. Image analysis of T cell clustering was performed using Incucyte S3 software. Analysis was stopped when cell density became too high to unambiguously identify clusters.

Cluster area quantification was performed using Top-Hat segmentation applied to the red fluroscent channel with a radius of 300 μm and a 0.4 RCU threshold. Thresholds for cluster area size and eccentricity were set at 1000 μm^2 and 0.7, respectively.

Confocal imaging of T cell clusters

Antigen-stimulated $CD8^+$ mTmG P14 T cells were grown for 48 h on fibronectin matrix-coated coverslips (Castelló-Cros and Cukierman, 2009). Then cells were fixed (2% PFA, 10 min, 37°C) and permeabilized (0.2% Triton X-100+1% BSA in PBS, 10 min, 22°C). After blocking (2% BSA in PBS, 10 min, 22°C) cells were first stained with biotinylated Anti-CTLA-4 (clone UC10-4B9, BioLegend) in 0.1% Tween, 1% BSA in PBS (1 h, 22°C) and then with Streptavidin-AlexaFluor488 (45 min, 22°C). Cells were mounted using mounting medium (Fluoromount-G, SouthernBiotech) containing 0.5 μg/mL DAPI (Sigma-Aldrich) and analyzed using a Cell Observer SD spinning disk confocal microscope (ZEISS). Image analysis and generation of 3D maximum intensity projections was performed using IMARIS software 8.3 (Bitplane, Oxford, UK).

Receptor-ligand pair prediction for T cells

To generate a library of receptors and corresponding ligands we merged information retrieved from 3 existing databases: Database of ligand-receptor partners (DLRP: http://dip.doe-mbi.ucla.edu/dip/DLRP.cgi) (Graeber and Eisenberg, 2001), human plasma membrane receptome (HPMR) (http://www.receptome.org/) (Ben-Shlomo et al., 2003) and the IUPHAR database (http://www.guidetopharmacology.org/linking.jsp) (Pawson et al., 2014). After mapping to official gene names, duplicates were excluded and genes listed were normalized to their corresponding murine homologs. This list was further curated by adding additional receptor ligand interaction derived from publications resulting in a library of 1465 interactions. We then developed an R-script interrogating gene expression datasets of naive and activated $CD8^+$ T cells for receptor-ligand pairs (i) for which both interactors are expressed by T cells, (ii) for which the expression levels of at least one interactor increases $\geq$ 2-fold upon T cell activation, and (iii) which are co-regulated across multiple infections (LCMV, *Listeria monocytogenes* and VSV) (GEO accession numbers: GEO: GSE30431, GEO: GSE15907). Each interaction identified by this algorithm was manually cross-checked using published literature to ensure that it truly denotes a receptor-ligand pair.

Mathematical model

Data accompanying the mathematical modeling is provided in the file "Data S1."

To understand the role of CD80 and CD86 in T cell expansion we constructed a dynamic mathematical model of the T cell population size which considers CD80- and CD86- induced CD28 signaling as well as IL-2R signaling. We aimed to include our findings that the population dynamics of T cells depends on the activity of the CD28 and IL-2R signaling pathways within an interacting T cell population. Instead of including a detailed representation of these pathways in the model, we split the T cell population into sub-populations of cells that are functionally different with respect to CD28 and/or IL-2R signaling, employing the flow cytometry and ELISA data as model inputs. This approach reduces the number of assumptions we need to make regarding the involved pathways and reduces the number of model parameters. Using ordinary differential equations (ODEs) we set up two models describing the T cell population: a three-compartment model that differentiates between divided (D) cells and two types of undivided (U) cells, i.e., undivided P14 TCR negative (U^-) and undivided P14 TCR positive (U^+) (Figure 5A) and a four-compartment model in which the divided cell compartment is subdivided into a CTLA-4 negative (D^-) and a CTLA-4 positive (D^+) compartment (Figure 5E).

In the *in vitro* experiments a fraction of the T cells do not carry a gp33-specific P14 TCR and, thus, will not recognize the peptide and die. We thus consider the undivided P14 TCR negative cell population to decline at a constant rate d_{U^-}:

$$\frac{dU^-(t)}{dt} = -d_{U^-} \cdot U^-(t)$$

The amount of gp33 remained sufficiently high to activate all P14 T cells during the experiment and therefore we did not explicitly represent antigen availability in our model. Undivided P14 TCR positive T cells either divide following activation (at a rate p_U) or die.

In all experiments, the total population size exhibits an initial dip, indicating that there is an initial period during which cells die but do not divide due to the experimental conditions. This is consistent with observations that the first T cell division events occur approximately one day post peptide infusion in *in vivo* settings (Mempel et al., 2004; Miller et al., 2004). Therefore, we incorporated a latent period ($0 < t < t_{latent}$) during which also undivided P14 TCR positive cells can only die. Because upon activation the P14 TCR positive cells start expressing the high affinity IL-2 receptor subunit CD25, we describe the death rate of undivided P14 TCR positive cells (D_{U^+}) as the difference of their basal death rate (d_{U^+}) and the effect of IL-2R signaling. Altogether, the dynamics of P14 TCR positive undivided cells are described by:

$$\frac{dU^+(t)}{dt} = \begin{cases} -d_{U^+} \cdot U^+(t) \text{ if } t \leq t_{latent} \\ -(D_{U^+}(t) + p_U) \cdot U^+(t) \text{ if } t > t_{latent} \end{cases}$$

For the stimulatory effect of IL-2 on survival, we consider a sigmoidal relation with the concentration of IL-2. This stimulation could fully prevent cell death, but is considered not to induce proliferation. The IL-2 signaling is scaled by the fraction of CD25 positive undivided cells because cells expressing CD25 at high levels are expected to respond much more strongly to IL-2 than cells with low CD25 surface expression. Thus:

$$D_{U^+}(t) = \max(d_{U^+} - CD25_U(t)s_{U,IL2R}H_{U,IL2R}(IL2(t)), 0)$$

Here, $CD25_U(t)$ is the interpolated fraction of CD25 expressing undivided cells, $s_{U,IL2R}$ is the maximum increase of expansion due to IL-2R signaling at high IL-2 concentrations, $IL2(t)$ the interpolated IL-2 concentration and H represents the Hill function $H_x(C) = (C^{n_x}/k_x^{n_x} + C^{n_x})$ with exponent n_x and saturation parameter k_x.

In the three compartment model (Figure 5B) the third compartment represents all divided cells (D) and grows or shrinks due to division of undivided P14 TCR positive cells and net expansion (i.e., taking into account division and death) of divided cells. The net expansion rate of divided cells is the summation of the, negative, basal expansion rate (p_D) and the expansion rate increase due to IL-2R ($P_{D,IL2R}(t)$). This gives rise to the following equation for divided cells:

$$\frac{dD(t)}{dt} = \left(p_D + P_{D,IL2R}(t)\right)D(t) + 2p_U \cdot U^+(t).$$

For the impact of IL-2R signaling on expansion, we assume the same sigmoidal relation as used for the undivided P14 TCR positive cells:

$$P_{D,IL2R}(t) = CD25_D(t)p_{D,IL2R}H_{D,IL2R}(IL2(t))$$

Here, $p_{D,IL2R}$ is the maximum increase of expansion due to IL-2R signaling at high IL-2 concentration and the fraction of CD25 expressing divided cells are interpolated from the *in vitro* data.

In the four compartment model, CD28 signaling is considered to promote division of already divided cells ($P_{D,CD28}(t)$) in the same manner as IL-2R signaling promotes such division ($P_{D,IL2R}(t)$). However, because there is a physical limit to how fast cells can pass through the cell cycle, we limited the increase of the divided cell expansion rate by the maximum increase of the expansion rate due to IL-2R signaling that is obtained at high IL-2 concentrations (i.e., $p_{D,IL2R}$). To include the inhibitory effect of CTLA-4 on CD28 signaling, we subdivide the divided cell compartment in a CTLA-4 negative (D^-) and a CTLA-4 positive (D^+) compartment (Figure 5E) and we describe the dynamics in these compartments by:

$$\frac{dD^-(t)}{dt} = \left(p_D + \min\left(P_{D^-,IL2R}(t) + P_{D,CD28}(t), p_{D,IL2R}\right) - R_{CTLA4+}(t)\right)D^-(t) + 2p_U \cdot U(t) + R_{CTLA4-}(t)D^+(t)$$

$$\frac{dD^+(t)}{dt} = \left(p_D + \min\left(P_{D^+,IL2R}(t) + P_{D,CD28}(t), p_{D,IL2R}\right) - R_{CTLA4-}(t)\right)D^+(t) + R_{CTLA4+}(t)D^-(t)$$

where $P_{D^-,IL2R}(t)$ and $P_{D^+,IL2R}(t)$ are similar to the equation defining $P_{D,IL2R}(t)$with $CD25_D$ substituted by $CD25_{D^-}$ and $CD25_{D^+}$, respectively. For CD28 induced expansion we assume a sigmoidal relation between the amount of cells expressing CD80 and/or CD86 and CD28 signaling output as well as a sigmoidal relation between the number of CTLA-4 positive cells and the inhibition of CD28 signaling:

$$P_{D,CD28}(t) = p_{D,CD28}H_{D,CD28}\left(N_{CD80/CD86}(t)\right) \cdot (1 - H_{D,CTLA4}(D^+(t)))$$

where $p_{D,CD28}$ is the maximum increase of the expansion rate due to CD28 signaling and $N_{CD80/CD86}(t)$ is the total number of CD80 or CD86 positive cells at time t:

$$N_{CD80/CD86}(t) = CD80/CD86_U(t)(U^-(t) + U^+(t)) + CD80/CD86_D(t)(D^-(t) + D^+(t)))$$

with $CD80/CD86_x(t)$ the fraction of CD80 or CD86 positive cells of type x:

$$CD80/CD86_x(t) = \min(CD80_x(t) + CD86_x(t), 1).$$

CTLA-4 expression and loss are modeled as the transition from D^- to D^- and vice versa, which occurs at rates $R_{CTLA4+}(t)$ and $R_{CTLA4-}(t)$. We consider CTLA-4 to be lost at a constant rate ($R_{CTLA4-}(t) = r_{CTLA4-}$), while gain of CTLA-4 expression occurs either at a constant rate ($R_{CTLA4+}(t) = r_{CTLA4+}$), or at a rate that depends on IL-2R signaling. For such IL-2R regulated CTLA-4 expression, we assume a sigmoidal relationship between IL-2 and the rate of CTLA-4 expression, which is scaled by the level of CD25 expression among the CTLA-4 negative divided cell population:

$$R_{CTLA4+}(t) = r_{CTLA4+}CD25_{D^-}H_{CTLA4+}(IL2(t)).$$

Here, r_{CTLA4+} represents the maximum rate of CTLA-4 expression at high IL-2 concentrations. A full list of the symbols used in all model variants can be found in Data S1, Table 1.

To identify the model parameter for which the model matches the *in vitro* experiment, we fit the model to the data for both WT and *Cd80*$^{-/-}$*Cd86*$^{-/-}$ cells. For the WT cells we simulate the full models as described above, and for the *Cd80*$^{-/-}$*Cd86*$^{-/-}$ cells $P_{D,CD28}$ is

set to zero. To initialize the models the total number of undivided cells is set to match the titrated cell count. The number of TCR P14 positive and negative cells are determined by a model parameter: $U^{+} = f_{P14+}U$ and $U^{-} = (1 - f_{P14+})U$. The model inputs, IL-2 concentrations, fractions of CD25 positive cells, and fractions of CD80 and/or CD86 positive cells, are obtained via interpolations from *in vitro* data Monotone Piecewise Cubic Interpolation (PCHIP) (Fritsch and Carlson, 1980) for each titration and well shape (see Figures 1–3 of Data S1).

We then fit the model to the *in vitro* data using least-squares fitting. Specifically, we use the, least_squares' function from the scipy optimization toolbox (Jones et al., 2001), which uses the Trust Region Reflective algorithm, in combination with the scipy's, solve_ivp' using the BDF implicit multi-step variable-order solver. Both the WT and *Cd80*$^{-/-}$*Cd86*$^{-/-}$ are included in a single fit by defining the following cost function:

$$F = \sum_{s}\sum_{t}\left(x_s^{WT}(t) - X_s^{WT}(t)\right)^2 + \sum_{s}\sum_{t}\left(x_s^{Cd80^{-/-}Cd86^{-/-}}(t) - X_s^{Cd80^{-/-}Cd86^{-/-}}(t)\right)^2$$

with $x_s^{WT}(t)$ and $x_s^{Cd80^{-/-}Cd86^{-/-}}(t)$ the values of model state variable s at time t and $X_s^{WT}(t)$ and $X_s^{Cd80^{-/-}Cd86^{-/-}}(t)$ the corresponding *in vitro* observations for respectively WT and Cd80$^{-/-}$Cd86$^{-/-}$ cells. Hence, after fitting we get a single parameter set that can describe both the WT and Cd80$^{-/-}$Cd86$^{-/-}$ cells. When fitting for multiple titrated cell counts, the cost function is extended to:

$$F = \sum_{n_0}\left(\sum_{s}\sum_{t}\left(x_s^{WT,n_0}(t) - X_s^{WT,n_0}(t)\right)^2 + \sum_{s}\sum_{t}\left(x_s^{Cd80^{-/-}Cd86^{-/-},n_0}(t) - X_s^{Cd80^{-/-}Cd86^{-/-},n_0}(t)\right)^2\right)$$

where n_0 refers to the number of titrated cells.

We ran the parameter fitting procedure for the three-compartment model and for the four-compartment model with either a constant rate of CTLA-4 expression or with IL-2 induced CTLA-4 expression. Note that we excluded the Hill coefficients from the fitting procedure because the model outcome hardly depends on the exact exponent in the Hill functions (data not shown). Rather, these exponents were fixed to the values listed in Table 2 in Data S1. Because the result of the fitting procedure strongly depends on the initial guess of the parameter values, we ran 5000 fits with varying initial guesses generated using latin hypercube sampling (McKay et al., 1979). The parameter values used for all the model fits shown are listed in Table 2 in Data S1. Note that while some proliferation rates may appear to be high, the lowest population doubling time we observed in the best-fitting simulations is over 4 h, which is not uncommon for T cells (Yoon et al., 2010).

QUANTIFICATION AND STATISTICAL ANALYSIS

Flow cytometry data was analyzed using FlowJo-software (BD Bioscience). Doublets and dead cells were excluded from analysis. Statistical analysis was performed using Prism 8 software (Graph Pad). The choice of statistical tests was based on normality testing and correction algorithms for multiple comparisons were applied when indicated. The following p value formatting was used: * $\leq$ 0.05, ** $\leq$ 0.01, *** < 0.001, **** < 0.0001. Plots depict mean ± standard deviation. For visualization purposes across experiments mean fluorescence intensities were normalized to appropriate negative controls (either knockout cells or "fluorescence minus one" samples). Statistical testing across experiments was performed on non-normalized MFIs using 2-way ANOVA. Figures were layouted using Inkscape software.

DATA AND CODE AVAILABILITY

Code developed for predicting candidate receptor-ligands pairs for quorum-regulation and mathematical modeling of T cell dynamics are available upon request.